FUNCTIONAL CHARACTERIZATION OF *RHOA* MUTATIONS IN PERIPHERAL T-CELL LYMPHOMAS

Ph.D. Thesis

Lucía Fernández Nevado

Centro de Investigación del Cáncer

Instituto de Biología Molecular y Celular del Cáncer

CSIC – Universidad de Salamanca

2023

Centro de Investigación del Cáncer
IBMCC - FICUS
(University of Salamanca-CSIC)
Miguel de Unamuno Campus
37007 Salamanca (Spain)
Tel.: (+34) 923 294720
www.cicancer.org

El **Dr. XOSÉ RAMÓN GARCÍA BUSTELO**, Profesor de Investigación del Consejo Superior de Investigaciones Científicas y el **Dr. JAVIER ROBLES VALERO**, Investigador Postdoctoral en el Centro de Investigación del Cáncer y el Instituto de Biología Molecular y Celular del Cáncer de Salamanca,

CERTIFICAN

Que el trabajo de tesis titulado **"Functional characterization of *RHOA* mutations in peripheral T-cell lymphomas"**, presentado por **Dª LUCÍA FERNÁNDEZ NEVADO** para optar al Grado de Doctor por la Universidad de Salamanca, ha sido realizado bajo mi dirección en el Centro de Investigación del Cáncer de Salamanca (USAL/CSIC). Considerando que cumple con las condiciones necesarias, autorizo su presentación a fin de que pueda ser defendido ante el tribunal correspondiente.

Y para que conste a los efectos oportunos, expido y firmo el presente certificado en Salamanca, a 14 de junio de 2023.

Fdo.: Dr. Xosé R. Bustelo

Fdo.: Dr. Javier Robles Valero

The research conducted in this Ph.D. thesis has been supported by:

i. Graduate student contracts from the Spanish Association against Cancer and from “la Caixa” Foundation (HR20-00164).

ii. The project leading to these results have received founding from “la Caixa” Foundation (HR20-00164), the Castilla-León autonomous government (CSI252P18, CSI145P20), the Spanish Ministry of Science and Innovation (RTI2018-096481-B-100), the Carlos III Health Institute (PI20/01724), and the Spanish Association against Cancer (GC16173472GARC).

iii. The ‘Programa de Apoyo a Planes Estratégicos de Investigación de Estructuras de Investigación de Excelencia’ of the Castilla–León autonomous government (CLC–2017–01).

“Es solo a través del trabajo y del esfuerzo doloroso,
con una energía siniestra y un coraje resuelto,
que avanzamos hacia cosas mejores”.
Theodore Roosevelt

ABSTRACT

RHOA is a small GTPase that belongs to the RHO proteins subfamily. During the last years, *RHOA* mutations have been identified in solid and hematological tumors. However, their pathobiological roles remain poorly characterized so far. In this thesis, we have functionally characterized these mutations, demonstrating that most of them lead to the inactivation of the GTPase activity of the protein. Focusing on the *RHOA* mutations described in peripheral T-cell lymphomas, we have proven that they activate the NFAT pathway independently of their canonical activity. This neomorphic activity is dependent on PLCγ1, SLP76, and LAT. Proteomic analyses identified RAP1GDS1as a key effector for the neomorphic function of RHOA mutants. The $RHOA^{G17V}$-driven tumors are sensitive to the pharmacological inhibition of NFAT activation. Altogether, our findings reveal novel pathobiological functions of RHOA and expand the current knowledge of the role of this protein in peripheral T-cell lymphomas. These data have unveiled an unexpected, neomorphic-like function of the RHOA mutants found in peripheral T-cell lymphomas. They also pinpoint new therapeutic opportunities for peripheral T-cell lymphoma patients.

TABLE OF CONTENTS

LIST OF FIGURES 13

LIST OF TABLES 16

LIST OF ABBREVIATIONS 19

INTRODUCTION 14

1. RHOA 15
   - 1.1. RHO GTPase subfamily 15
   - 1.2. Structure and regulatory cycle 15
   - 1.3. Posttranslational modifications 17
   - 1.4. Transcriptional and post-transcriptional regulation of *RHOA* 19
   - 1.5. RHOA interactors and effectors 19
   - 1.6. Cellular, physiological, and pathological functions 22
   - 1.7. RHOA in cancer 24
     - 1.7.1. *RHOA* mutations in cancer 25

2. PERIPHERAL T-CELL LYMPHOMAS 33
   - 2.1. T lymphocytes 33
   - 2.2. T cell receptor complex 34
   - 2.3. T cell receptor signaling 35
   - 2.4. Peripheral T-cell lymphomas 37
     - 2.4.1. Pathogenesis 38
   - 2.5. Angioimmunoblastic T cell lymphoma 40
     - 2.5.1. Clinical presentation and pathogenesis 40
     - 2.5.2. Mutational landscape of angioimmunoblastic T cell lymphomas 41
     - 2.5.3. Treatment 43

OBJECTIVES 45

METHODS 49

RESULTS 66

1. CHARACTERIZATION OF TUMOR-ASSOCIATED *RHOA* MUTATIONS 68

1.1. Most RHOA mutants modify the canonical activity of the protein 68

1.2. PTCL-related RHOA mutants display a neomorphic function 69

1.3. Extracellular calcium is essential for NFAT activation by RHOA neomorphic mutants..... 74

2. RHOA NEOMORPHIC MUTANTS ACTIVATE THE NFAT PATHWAY THROUGH THE INTERACTION WITH THE PLCγ1-SIGNALOSOME ... 76

2.1. Neomorphic mutants use LAT, PLCγ1, and SLP76 but not VAV1 for NFAT activation 76

2.2. The neomorphic mutants RHOA^{C16R} and RHOA^{G17V} form a complex with the proteins PLCγ1, VAV1, AND SLP76..... 76

3. RAP1GDS1 MEDIATES RHOA NEOMORPHIC EFFECT 80

3.1. Proteomic analyses identified a specific effector for RHOA neomorphic mutants..... 80

3.2. RHOA neomorphic mutant proteins specifically bind to RAP1GDS1 and lose the interaction WITH RHOGDIα..... 80

3.3. RAP1GDS1 is essential for NFAT activation elicited by RHOA NEO mutants..... 84

3.4. Role of the CAAL domain of non-NEO mutant RHOA^{R5W} for NFAT activation and implication of RAP1GDS1 and RHOGDIα..... 91

4. ROLE OF *RHOA* NEOMORPHIC MUTATIONS *IN VIVO*..... 93

4.1. NEO+LOF mutants enhance proliferation in mouse CD4^{+} T cells when combined with *Tet2* loss 93

4.2. RAP1GDS1 is important for the *in vivo* effects of RHOA neomorphic mutants..... 95

4.3. Oncogenic driver role of RHOA^{G17V} on PTCL formation..... 97

4.4. RHOA^{G17V}-driven lymphomagenesis is NFAT-dependent..... 99

DISCUSSION..... 109

CONCLUSIONS..... 66

BIBLIOGRAPHY..... 70

ACKNOWLEDGMENTS..... 139

APPENDIX..... 90

Resumen en español..... 90

LIST OF FIGURES

Figure 1. **The RHO GTPase family** 15

Figure 2. **RHOA structure** 16

Figure 3. **The RHO GTPase activation cycle** 17

Figure 4. **Posttranslational modifications in RHOA** 18

Figure 5. **Known regulators of RHOA** 20

Figure 6. **Schematic summary of the known RHOA effectors and functions** .. 23

Figure 7. ***RHOA* mutations found in human tumors** 26

Figure 8. **Consequences of mutations on RHOA GDP-GTP regulation and effector interaction** 28

Figure 9. **TCR complex** 34

Figure 10. **Main TCR signaling pathways.** 37

Figure 11. **T helper cell lineages and their connection with PTCL development** 38

Figure 12. **Schematic representation of AITL development** 42

Figure 13. **Functional impact of RHOA mutations in the canonical activity of the protein** 69

Figure 14. **Effect of *RHOA* mutations in the activation of STAT3, NOTCH1, AP-1, and NF-κB pathways** 70

Figure 15. **PTCL-related *RHOA* mutations display a neomorphic effect** 72

Figure 16. **Effect of RAC1 and CDC42 on the activation of the NFAT pathway** 74

Figure 17. **Extracellular calcium is essential for NFAT activation by the NEO mutations** 75

Figure 18. **NEO mutations need PLCγ1-signalosome proteins to activate the NFAT pathway**. 78

Figure 19. **RHOA^{C16R} and RHOA^{G17V} NEO mutants interact with the PLCγ1-signalosome proteins PLCγ1, VAV1 and SLP76** 78

Figure 20. **The RHOA^{C16R}-PLCγ1-VAV1-SLP76 complex** 79

Figure 21. **Identification of a NEO effector by proteomic analyses** 81

Figure 22. **NEO mutations exhibit strong interaction with RAP1GDS1 and lose the interaction with RHOGDIα.** 82

Figure 23. **RAP1GDS1 interaction with NEO mutants is RHOA-specific** 83

Figure 24. **Generation of Jurkat cells containing short hairpins for RAP1GDS1** 84

Figure 25. **RAP1GDS1 is essential for the activation of NFAT by the NEO mutations** 86

Figure 26. **RHOA double mutants impair NFAT activation when not interacting with RAP1GDS1** 87

Figure 27. **Effect of the CAAL domain alteration in NFAT activation and interaction with RAP1GDS1** 89

Figure 28. **Non-neomorphic mutants activate NFAT when the interaction with RHOGDIα is lost and the interaction with RAP1GDS1-607 is increased** 92

Figure 29. ***RHOA* NEO mutations alone do not drive proliferation of mouse CD4$^+$ T cells** 93

Figure 30. **NEO+LOF *RHOA* mutations combined with Tet2 loss promote proliferation in mouse CD4$^+$ T lymphocytes.** 95

Figure 31. **Impact of the RAP1GDS1-RHOA interaction in primary T cells**.... 97

Figure 32. **Analysis of the effect in vivo of mice transplanted with *Tet2*$^{-/-}$ CD4^{+} T cells expressing RHOA NEO mutations** 99

Figure 33. **Analysis of the effect of NFAT inhibition in recipient mice containing RHOA^{G17V}-expressing CD4^{+} T cells** 101

Figure 34. **Histopathologic analysis of the effect of NFAT inhibition in recipient mice transplanted with RHOA^{G17V}-expressing CD4^{+} T cells**. 104

Figure 35. ***In vitro* effect of different anti-tumoral drugs in RHOA^{G17V}-deribed PTCL cells**..... 106

LIST OF TABLES

Table 1. ***RHOA* mutations described in human tumors** 30

Table 2. **Primers used for the generation of *RHOA* mutations by site-directed mutagenesis** 51

Table 3. **Primary antibodies used for expression analyses** 55

Table 4. **Primers used for gene expression analyses** 58

Table 5. **Antibodies used for flow cytometry determination** 61

LIST OF ABBREVIATIONS

AC	Adenocarcinoma
ADAP	Adhesion and Degranulation-promoting Adaptor Protein
AITL	Angioimmunoblastic T cell lymphoma
AKT	Protein kinase B
ALCL	Anaplastic T-cell lymphoma
ALK	Anaplastic Lymphoma Kinase
AMP	Adenosine Monophosphate
AP-1	Activating Protein-1
ARP2/3	Actin-Related Proteins-2/3
ATLL	Adult T-cell leukemia/lymphoma
ATP	Adenosine triphosphate
BCL6	B-cell lymphoma 6
BCL10	B cell lymphoma 10
BSA	Bovine Serum Albumin
CDC42	Cell Division Control protein 42
CD3	Cluster of differentiation 3
CD4	Cluster of differentiation 4
CD8	Cluster of differentiation 8
CD28	Cluster of differentiation 28
CDC42	Cell Division Control protein 42
cDNA	Complementary DNA
CTCL	Cutaneous T cell lymphoma
CTLA4	Cytotoxic T-Lymphocyte Associated Protein 4
CTNNB1	Catenin beta 1
CXCL13	C-X-C Motif Chemokine Ligand 13
CXCR5	C-X-C Motif Chemokine Receptor 5
DBL	Diffuse B-cell lymphoma
DMEM	Dulbecco´s modified Eagle's medium
DMSO	Dimethyl Sulfoxide
DNA	Deoxyribonucleic acid
ECT2	Epithelial Cell Transforming 2
EGF	Epithelial growth factor
EGFP	Enhanced Green Fluorescent Protein
EGTA	Egtazic acid
ERG	Ether-a-go-go Related Gene
ERK1/2	Extracellular signal-regulated kinase 1/2
FACS	Fluoresce-Activated Cell Sorting
FBS	Fetal Bovine Serum
FOXP3	Forkhead box protein P3
GADS	GRB2-related adaptor downstream of Shc
GAP	Guanosine Activating Protein
GATA3	GATA binding protein 3
GDI	Guanosine Dissociation Inhibitor
GDP	Guanosine diphosphate
GEF	Guanosine Exchange factor
GMP	Guanosine Monophosphate
GOF	Gain-of-function
GRB2	Growth factor receptor-bound protein 2

GSK3	Glycogen Synthase Kinase 3
GST	Glutathione S-transferase
GTF2I	General Transcription Factor IIi
GTP	Guanosine triphosphate
HES1	Hes Family BHLH Transcription Factor 1
Icmt	Isoprenylcysteine Carboxyl Methyltransferase
ICOS	Inducible T-cell costimulatory
IFN-γ	Interferon gamma
IKK	IkappaB Kinase
IL-2	Interleukin 2
IL-4	Interleukin 4
IL-5	Interleukin 5
IL-6	Interleukin 6
IL-10	Interleukin 10
IL-13	Interleukin 13
IL-17A	Interleukin 17A
IL-17F	Interleukin 17F
IL-21	Interleukin 21
IL-22	Interleukin 22
IP	Immunoprecipitation
ITK	IL-2-inducible T cell Kinase
JAK	Janus Kinase
JNK	c-Jun N-terminal kinase
LARG	Leukemia-associated RHO GEF
LAT	Linker for Activation of T cells
LCK	Lymphocyte-specific protein tyrosine kinase
LDH	Lactate dehydrogenase
LOF	Loss-of-function
MALT1	Mucosa-associated Lymphoid Tissue Lymphoma Translocation protein 1
MAPK	Mitogen-activated protein kinase
MEK	Mitogen-activated protein kinase kinase ½
MHC	Major histocompatibility complex
miRNA	Micro RNA
mTOR	mammalian target of Rapamycin
n	Number of experimental replicates
NCK	Non-catalytic region of tyrosine kinase adaptor protein
NEO	Neomorphic
NFAT	Nuclear Factor of Activated T cells
NF-κB	Nuclear factor kappa-light-chain-enhancer of activated B cells
NKTCL	Natural Killer/T cell lymphoma
NIK	NF-κB-inducing kinase
NK	Natural Killer
NOTCH1	Neurogenic locus notch homolog protein 1
NSCLC	Non-small cell lung cancer
NSG	NOD scid gamma mouse
ORAI1	Calcium release-activated calcium channel protein 1
PBS	Phosphate-buffered saline
PCR	Polymerase Chain Reaction
PD1	Programmed cell death protein 1
PDK1	Pyruvate Dehydrogenase Kinase 1)
Pi	Inorganic phosphate
PI3K	Phosphoinositide 3-kinase
PKCθ	Protein Kinase C theta
PLCγ1	Phospholipase C gamma 1
PTCL	Peripheral T-cell lymphoma

PTCL-NOS	**Peripheral T-cell lymphoma- not otherwise specified**
RAC1	**Ras-related C3 botulinum toxin substrate 1**
RAF1	**Proto-oncogene serine/threonine-protein kinase 1**
RASGRP1	**Ras guanyl-releasing protein 1**
RBD	**Rho binding domain**
Rce1	**Ras converting CAAX endopeptidase 1**
RHOA	**Ras Homolog family member A**
RNA	**Ribonucleic acid**
ROR-γt	**RAR-related Orphan Receptor gamma**
rpm	**Revolutions per minute**
RT-PCR	**Reverse-transcription polymerase chain reaction**
SAP	**Serum Amyloid P component**
SCC	**Squamous cell carcinoma**
SLP76	**Src homology 2 domain containing leukocyte protein 76**
SOS	**Son of Sevenless**
SPAK	**Ste20/SPS1 related proline and alanine rich kinase**
SRF	**Serum response factor**
STAT	**Signal Transducer and Activator of Transcription**
TAZ	**Tafazzin family protein**
TBS-T	**Tris-buffered saline and Tween 20**
TBX21	**T-box Transcription Factor 21**
TCR	**T cell receptor**
TGF-β	**Transforming growth factor beta**
VEGF	**Vascular Endothelial Growth Factor**
WASP	**Wiskott–Aldrich syndrome protein**
WAVE2	**WASP-family verprolin-homologous protein 2**
WHO	**World Health Organization**
WT	**Wild type**
YAP	**Yes-associated protein**
ZAP-70	**Zeta-chain of TCR-associated protein 70**

INTRODUCTION

1. RHOA

1.1. RHO GTPASE SUBFAMILY

RHOA is a small GTPase that belongs to the RHO GTPase family of RAS-related superfamily and is found in nearly all eukaryotic cells [1, 2]. The human RHO GTPase family consists of 20 members and can be classified into 8 subfamilies based on their homology and structure. Moreover, they can be divided into typical or atypical GTPases depending on their regulation [2, 3] (**Figure 1**).

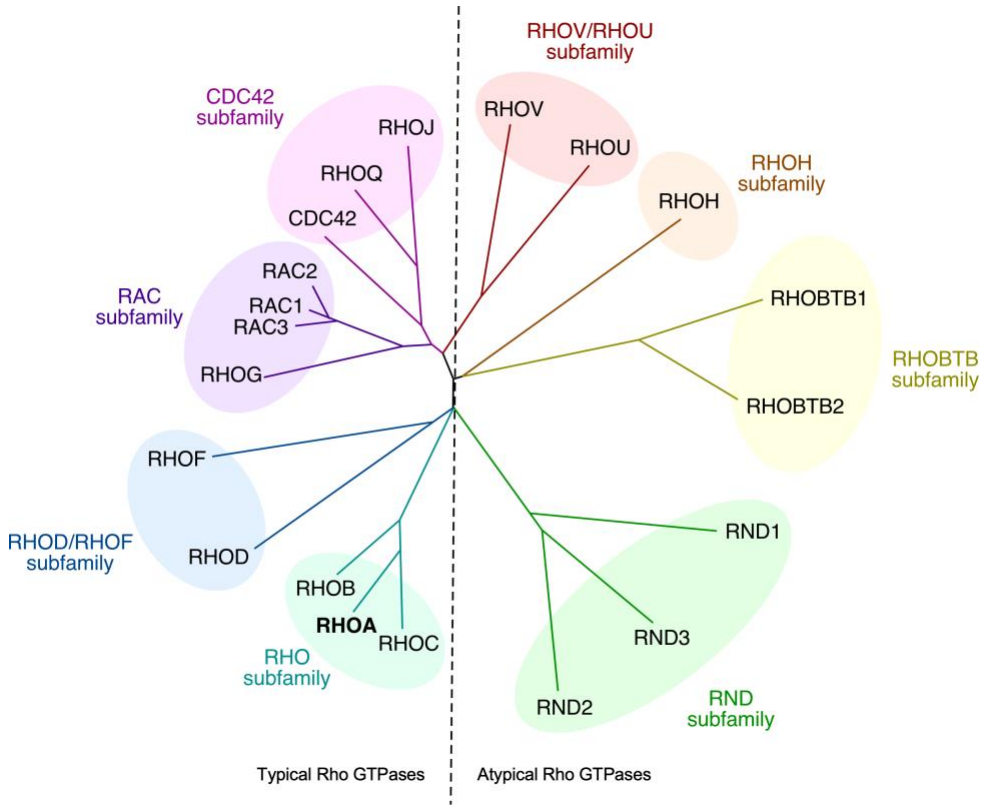

Figure 1. The RHO GTPase family. The RHO GTPase family consist of 20 proteins divided into the following subfamilies: RAC, RHO, RHOD/RHOF, RND, RHOBTB, RHOH, CDC42 and RHOV/RHOU. These subfamilies can be classified into typical (left) or atypical (right) based on their mode of regulation. Figure modified from [3].

1.2. STRUCTURE AND REGULATORY CYCLE

RHOA is a monomeric protein that contains 193 amino acids and a molecular weight of 21.7 kDa. It possesses several key domains, including the “G box” domain, an insert

domain, and a terminal hypervariable domain (**Figure 2**). The G box domain is composed by five highly conserved sequence motifs (G1 to G5) that are directly involved in the binding of the guanine nucleotides (G1), the reorientation of all the components to facilitate the binding of the effectors (G2), the binding of the nucleotide-associate Mg^{2+} ions (G3), the specificity to GTP over ATP (G4), and the stabilization of the complex (G5) [4]. The switch I and switch II domains, which sense whether a GTP or GDP molecule is bound, respectively, are also part of the G2 and G3 motifs, and they change their conformation accordingly in a process known as 'loading-spring' mechanism [5]. Most of the residues involved in GTP binding, stabilization or regulation of the hydrolysis reaction are located in this domain, including Gly^{14}, Thr^{19}, Phe^{30}, and Gln^{63} residues, and are highly conserved among the three RHO isoforms. Furthermore, other conserved amino acids serve as targets for bacterial toxins, such as Asn^{41} (*Clostridium botulinum* exoenzyme C3 transferase) or Thr^{37} (*Clostridium difficile* Toxin B), suggesting an important role of these residues in protein regulation [6, 7] (**Figure 2**). The RHO insert region, a hallmark of all members of the RHO GTPase family, is located between the G4 and G5 motifs, in the residues 123 to 137. It determines the binding of the GTPase to different effector proteins [5, 7]. Finally, the hypervariable domain partially determines specific binding to regulatory and effector proteins, as it functions as a protein binding site. Moreover, it contains the CAAX domain, which is essential for proper protein localization [5-7].

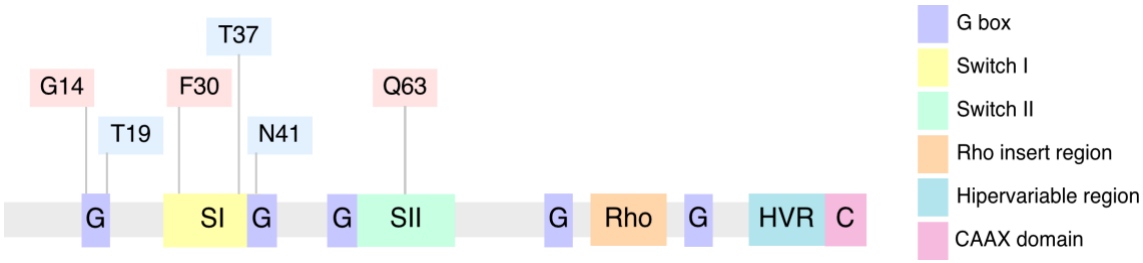

Figure 2. RHOA structure. Schematic representation of the RHOA protein highlighting the localization of its different domains and key residues that play important roles in its function. Mutations of these residues have been used to generate constitutively active (light red) or dominant negative (light blue) proteins.

Regarding its mode of action, RHOA is a molecular switch that fluctuates between an active GTP-bound state and an inactive GDP-bound state. This cycle is tightly regulated by the coordinated action of different proteins. Guanine nucleotide exchange factors (GEFs) catalyze the exchange of GDP for GTP, activating the GTPase, whereas

GTPase activating proteins (GAPs) increase the rate of GTP hydrolysis, promoting the inactivation of the GTPase. A second layer of regulation is provided by guanine nucleotide dissociation inhibitors (GDIs), which sequester GDP-bound GTPases in the cytosol, preventing their activation by GEFs or their localization to the plasma membrane [2, 8-10] (**Figure 3**). Upon activation, RHO GTPases undergo conformational changes that enhance their ability to interact and activate downstream effector molecules (**Figure 3**). This ultimately regulates a variety of cellular processes which vary depending on the specific stimulus and cell type. Some of them include cell cycle progression, gene expression, vesicle transport, migration, morphogenesis, neuronal development, cell division, adhesion, reactive oxygen species (ROS) production, and glucose homeostasis [1, 3, 11, 12].

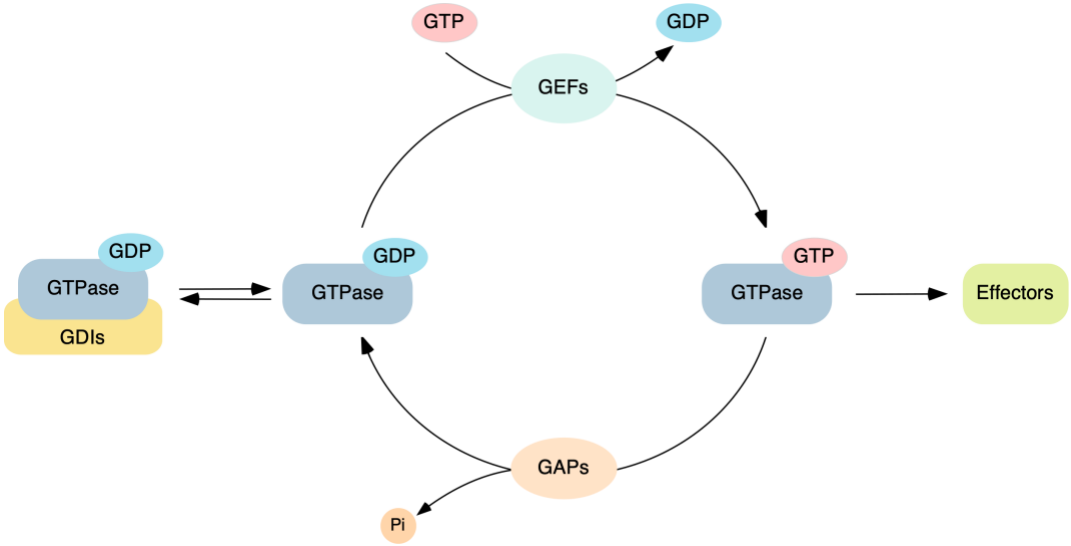

Figure 3. The RHO GTPase activation cycle. Representation of the mechanism of activation and deactivation of GTPases and the regulators involved in the process. Pi: inorganic phosphate; GDP, guanosine diphosphate; GTP, guanosine triphosphate.

1.3. POSTTRANSLATIONAL MODIFICATIONS

RHOA undergoes posttranslational lipid modifications at its CAAX domain (**Figure 4**). Particularly, RHOA is geranylgeranylated at the cysteine residue of the CAAX domain in a process catalyzed by type I geranyl-geranyl transferase in the cytoplasm. The addition of this isoprenoid group promotes the translocation of the protein to the endoplasmic reticulum, where the last three amino acids of the CAAX domain are then removed by

the protease Rce1. Following this cleavage, Cys^{190} is methylated by the carboxyl methyltransferase Icmt [9].

In addition to this carboxyl-terminal modification, the residues Lys^{6}, Lys^{7}, and Lys^{51} of RHOA can be ubiquitinated by the ubiquitin ligase Smurf1. In addition, the Lys^{135} residue can be ubiquitinated by the BACURD-cullin3 complex (**Figure 4**). Finally, GDP-RHOA and GTP-RHOA are substrates of FBXL19 E3 ubiquitin ligase. All these mechanisms result in the degradation of RHOA by the proteasome [2, 5, 6, 13]

Phosphorylation of the residues Ser^{188}, Ser^{26}, Tyr^{34}, and Tyr^{66} by different kinases such as Protein Kinase A (PKA), cyclic GMP-dependent protein kinase (PKG), Cbr-Abl and Scr, leads to the inactivation of RHOA and its localization in the cytoplasm bound to RHOGDI [5, 8, 14, 15]. On the contrary, phosphorylation at residues $Ser^{188,}$ Thr^{177}, and Thr^{100} by Protein Kinase C delta (PKCδ) or ERK can promote its activation [16]. Moreover, phosphorylation at Tyr^{42} has opposite effects: SRC-mediated phosphorylation promotes RHOA activation [17], whereas the phosphorylation mediated by c-Met leads to RHOA degradation by the proteosome [18] (**Figure 4**).

RHOA can also undergo posttranslational modifications such as nitrosylation, adenylation, oxidation, or transglutamination (**Figure 4**). The addition of a nitro group on Tyr^{34} leads to the activation of RHOA [19], whereas Tyr^{34} adenylation results in RHOA inhibition [20]. Cys^{16} and Cys^{20} can be oxidized by reactive oxygen species (ROS), leading to the inactivation of RHOA [21]. However, when combined with Tyr^{42} phosphorylation, the oxidation of these residues promotes the activation of RHOA [17]. Finally, the residue Gln^{63} can bear different types of transglutamination, promoting permanent activation of RHOA [22, 23].

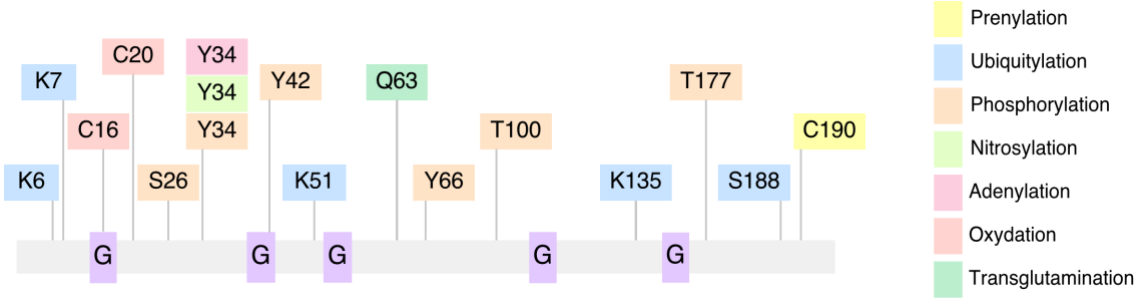

Figure 4. Posttranslational modifications in RHOA Scheme showing RHOA residues that undergo prenylation, ubiquitylation, phosphorylation, nitration, adenylation, oxidation, and transglutamination.

1.4. TRANSCRIPTIONAL AND POST-TRANSCRIPTIONAL REGULATION OF *RHOA*

RHOA is expressed in virtually all tissues [7]. *RHOA* expression is controlled by several transcription factors and complexes, such as the Myc-Skp2-Miz1-p300 complex, hypoxia-inducible factor 1 alpha (HIF-1α), signal transducer and activator of transcription 6 (STAT6), nuclear factor-κB (NF-κB) and activating transcription factor 1 (ATF-1). Besides, the CCAAT box in the promoter of *RHOA* is a binding site for transcription factors such as binding protein beta (CEBPB) and delta (CEBPD), nuclear factor Y A (NFYA), and B (NFYB) [6, 24, 25].

Post-transcriptionally, *RHOA* expression can be regulated by numerous miRNAs in response to different stimuli in specific cells. For instance, miR-155, miR-31, miR-122, miR-125a-3p, miR-146a, miR-133b, miR-185, miR-340, and miR-142 have been identified as regulators of *RHOA* gene [2, 24-26].

1.5. RHOA INTERACTORS AND EFFECTORS

In humans, more than 80 GEFs, 70 GAPs and 3 GDIs have been identified for RHO GTPases proteins [2, 11, 27, 28]. Regarding RHOA, numerous interactions with GEFs, GAPs, and GDIs have been identified through diverse *in vitro* studies using murine and human cell lines (**Figure 5**).

RHO GEFs serve as critical signaling nodes, connecting multiple kinase-mediated signaling cascades to the regulation of RHOA. While most of the GEFs function across different GTPases, there are specific GEFs identified for RHOA. Notably, examples of RHOA-specific GEFs include Leukemia-associated RHO GEF (LARG), p115, and PDZ-RHOGEF, which are selectively regulated by $G\alpha_{12/13}$ heterotrimeric G-proteins, thus providing a link between activated G-protein-coupled receptors (GPCRs) coupled to $G\alpha_{12/13}$ and the RHOA signaling [29].

A recent study also reported that the nucleotide-free $RHOA^{G17A}$ protein interacts with the RHOA-specific GEFs ARHGEF1, ARHGEF2, ARHGEF5, ARHGEF17, NGEF29, ECT2, and AKAP13. However, there are GEFs that demonstrate less specificity for RHOA and interact with both RAC1 and/or CDC42. These GEFs include

VAV1, VAV2, TRIO, ARHGEF11, ARHGEF12, PLEKHG3, FARP1, and BCR [30] (**Figure 5**).

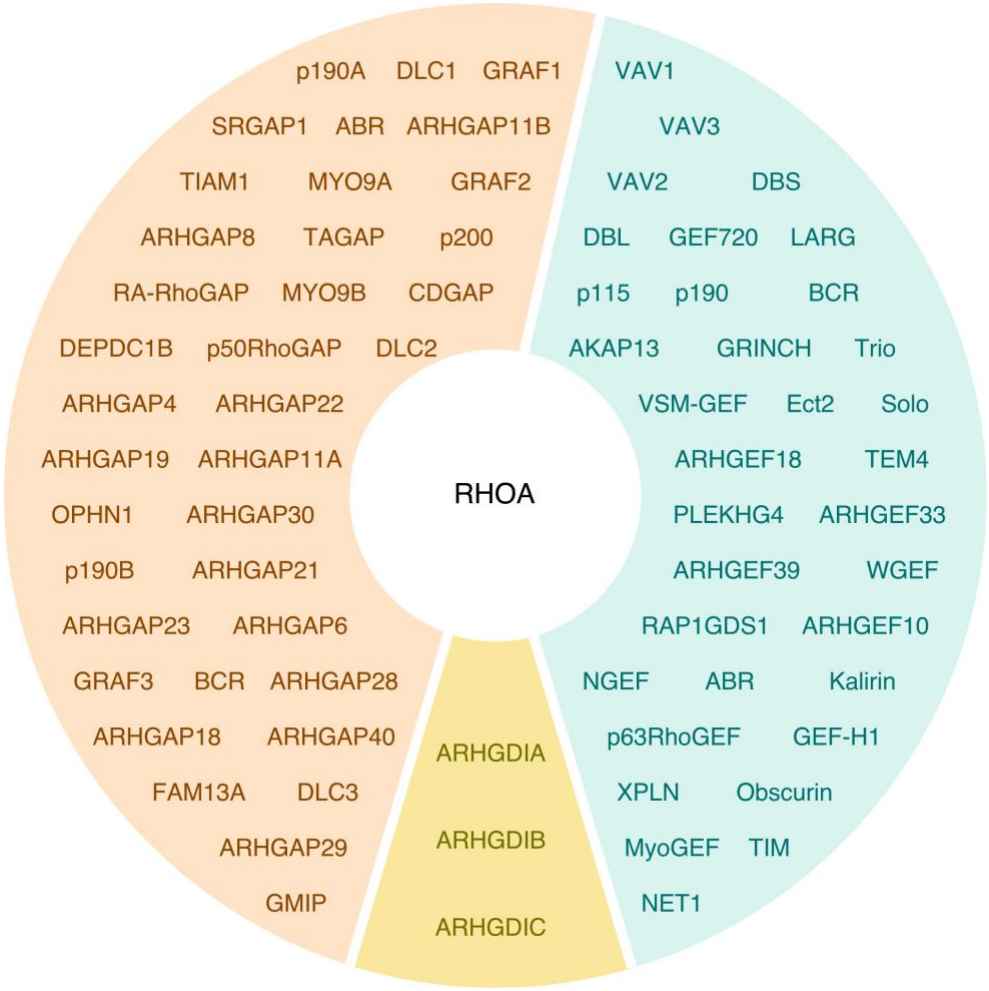

Figure 5. Known regulators of RHOA. Scheme showing the GEFs (mint), GAPs (orange), and GDIs (yellow) that have been reported to regulate RHOA activity.

In addition to the mentioned GEFs, there is a group of atypical GEFs, including RAP1GDS1, that interact with RHOA. Unlike GEFs of the DBL and DOCK families, RAP1GDS1 is exclusively composed of armadillo-repeat motifs [31, 32]. Moreover, it widely interacts with small GTPases from the RAS and RHO families [33]. However, recent studies have shown that it functions exclusively as a GEF for RHOA and RHOC [34]. This protein has two splice variants, RAP1GDS1-607 and RAP1GDS1-558, which only differ in the presence of an armadillo motif in their structure [35]. RAP1GDS1 also acts as a chaperone that controls prenylation and intracellular trafficking of GTPases.

RAP1GDS1-607 binds to non-prenylated small GTPases and allows their entry to the prenylation pathway, whereas RAP1GDS1-558 binds to prenylated small GTPases [36].

Regarding RHO GAPs, they are characterized by a highly conserved RHO GAP domain that mediates the binding to GTP-bound RHO proteins and stimulates their intrinsic GTPase activity [37]. These proteins exhibit a promiscuous nature, being poorly specific towards different RHO GTPases. Recent studies using the constitutively active form $RHOA^{G14V}$ have confirmed evidence for the specific interaction between RHOA and RHO GAPs. Examples of RHOA-specific interactions include MYO9A, MYO9B and ARHGAP29, whereas other GAPs display broad interaction patterns with other RHO GTPases, such as ARHGAP1, ARHGAP5, ARHGAP21, ARHGAP32, or ARHGAP39, among others [30] (**Figure 5**).

Unlike GEFs and GAPs, the RHO GDI family is comprised of only 3 members: RHOGDIα, RHOGDIβ, and RHOGDIγ. These proteins have a key role in the negative regulation of RHO GTPases, inhibiting the GTPase activity of RHO proteins by preventing their interaction with GEFs [38]. Specifically, RHOA has been described to interact with RHOGDIα and RHOGDIγ in HEK293T cells [39], as well as with RHOGDIβ in T cells [40-42] (**Figure 5**).

Interestingly, apart from the classical RHO GTPase regulators, the RHO family interacting cell polarization regulators (RIPORs) have been demonstrated to be novel partners of the RHO subfamily members. This family of proteins is comprised of three members: RIPOR1 or FAM65A, RIPOR2 or FAM65B, and RIPOR3 or FAM65C. These proteins bind directly to RHOA through a RHO-binding domain, and exert suppressive effects on RHO activity. For example, RIPOR2 binds to RHOA, reducing RHOA-mediated transcriptional activation and suppressing T cell and neutrophil migration [43].

Upon activation, RHOA exerts its cellular functions by binding with a plethora of downstream effectors. The switch domains of RHOA interact with the Rho-binding domain (RBD) present in effector proteins, leading to the loss of intramolecular autoinhibitory interactions and exposure of functional domains in the effectors [6]. These molecules can be divided into two different classes: serine/threonine protein kinases such as RHO-associated coiled-coil kinase (ROCK), citron kinase, and protein kinase N (PKN), and scaffold proteins such as mammalian diaphanous-related formin (mDia),

rothekin, kinectin, and rhophilin [37]. Recently, the landscape of RHO GTPase effectors has been renewed, revealing both stablished RHOA effectors and novel specific ones. These newly identified RHOA effectors include the kinases SLK and STK10, heme oxygenase (HMOX2), Elkin1, the B cell receptor associated protein 31 (BCAP31), the Fas-associated factor family member 2 (FAF2), Sec1 family domain-containing protein 1 (SCFD1), ER Membrane Protein Complex Subunit 3 (EMC3), Aladin, Formin Like 3 (FMNL3), YKT6 V-SNARE homolog, and ATPase H^+ Transporting Accessory Protein 1 (ATP6AP1). However, it is important to note that the specific interactions between RHOA and many of these effectors still require further verification [30].

1.6. CELLULAR, PHYSIOLOGICAL, AND PATHOLOGICAL FUNCTIONS

RHOA was initially shown to participate in the cytoskeleton dynamics, specifically in the regulation of stress fibers and focal adhesion complexes formation, which controls cell shape, polarity, cell-cell interactions, cell movement, and invasion [1, 7]. Moreover, RHOA plays an important role in cytokinesis by promoting the formation and stabilization of the contractile ring and the correct orientation of the spindle [44, 45] (**Figure 6**).

Subsequent studies demonstrated that RHOA also participates in other cytoskeleton-dependent cellular processes. RHOA is responsible for Golgi morphology and its reorientation towards the leading edge of the cell, the formation of dendritic Golgi outposts in neurons, and the generation of Rab6-positive vesicles derived from the Golgi apparatus [46, 47]. In line with this, RHOA is also implicated in the vesicular trafficking of the cell, including processes such as clathrin-dependent and -independent endocytosis, phagocytosis, and regulated exocytosis [48]. Moreover, it promotes cell cycle progression through the expression and activation of the cyclin D1, the downregulation of p21, and the degradation of p27 [49]. Furthermore, RHOA regulates gene transcription, including the serum response factor (SRF), the JNK and p38 MAPK pathway, NF-κB, YAP/TAZ, and STAT3 [1, 24]. Finally, RHOA regulates enzymes associated to the lipid metabolism and the generation of lipid second messengers such as phosphatidylinositol 4,5-bisphosphate (PIP2) or phosphatidic acid (PA) [50], as well as several ion channels, including the epithelial Na^+ channel, the potassium voltage-gated channel ERG, or Kv1.2 channels, among others [51].

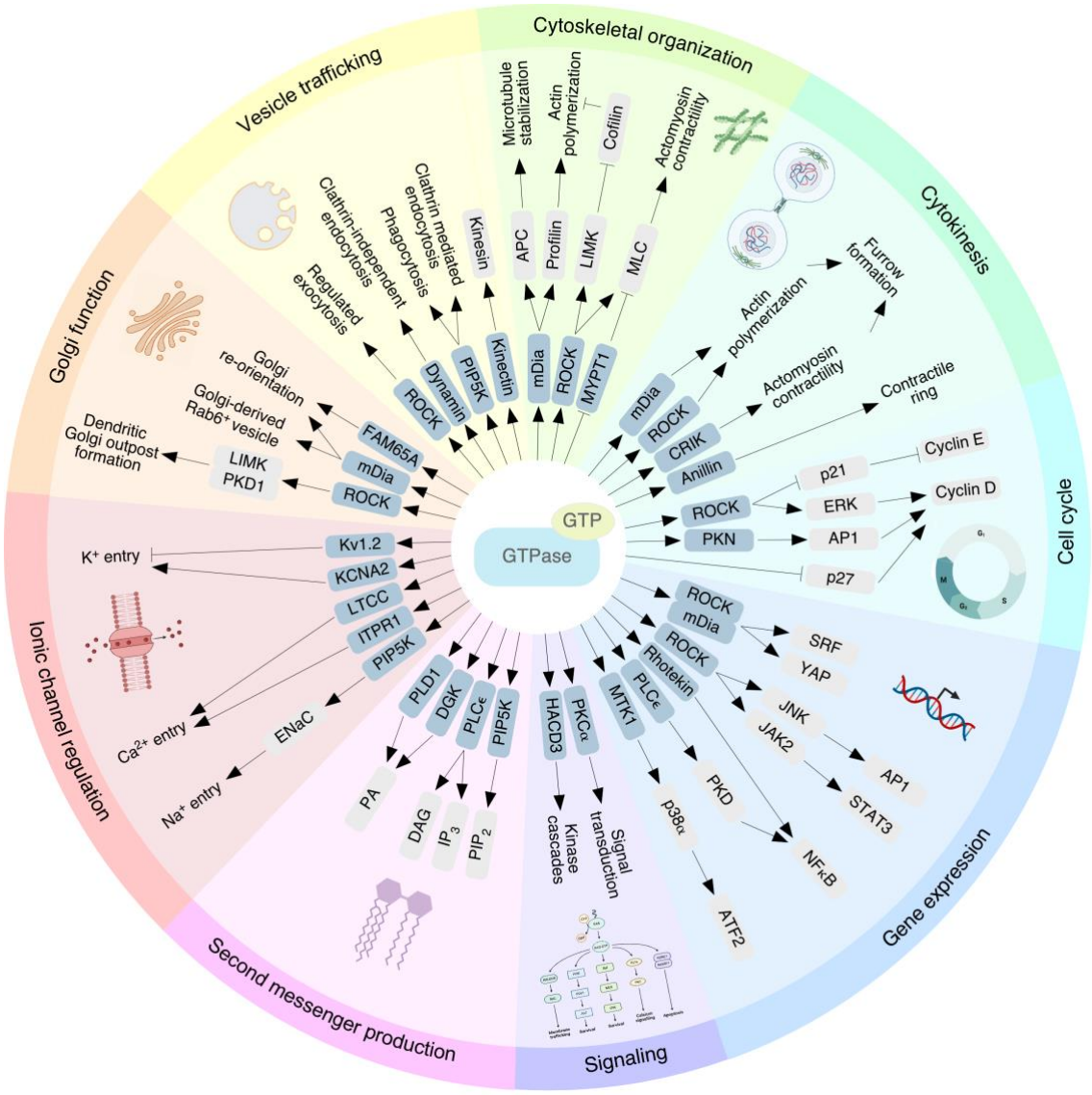

Figure 6. Schematic summary of the known RHOA effectors and functions. Scheme summarizing the main cellular functions performed by RHOA along with its effectors (dark grey) and the proteins involved (light grey). Some effectors overlap several functions.

Apart from the functions mentioned above, RHOA also has specialized roles, including neuronal apoptosis and morphology [52], axon branching and axonogenesis [53], microglial function [54], mitochondrial movement [55], angiogenesis [56], or regulation of innate and adaptive immunity [57].

Furthermore, the use of gene-targeted technology has allowed to gain further insight into the roles of RHOA *in vivo*. *Rhoa* null knockout mice have been reported to die during embryological development [58], indicating a critical role of RHOA in an early stage of development. *RhoA* conditional knockout models in different organs have

demonstrated the role of RhoA in skin development and maintenance, eye development, cardiovascular regulation, neural development, and regulation of the hematolymphoid system [59].

1.7. RHOA IN CANCER

Given its involvement in vital cellular and biological processes, the deregulation of RHOA has been associated with a wide range of pathological conditions. These include neurodegenerative diseases [26], vascular [60] and cardiovascular diseases [61], immune-mediated diseases [57], and tumorigenesis [62]. Indeed, RHOA has been implicated in nearby all stages of tumorigenesis, encompassing oncogenic transformation, inhibition of apoptosis, metabolic switch, promotion of cancer stemness, survival, inflammation, proliferation, angiogenesis, invasion, and metastasis [63]. Furthermore, *RHOA* is frequently overexpressed in various tumor types, including breast cancer, colon cancer, lung cancer, or squamous cell carcinoma, among others. Such overexpression is often associated with a poor prognosis [62]. These data strongly support the notion that RHOA acts as an oncogene in different tumor types through its participation in different stages of tumorigenesis.

However, recent findings are challenging the conventional view that considers RHOA exclusively as an oncogene. Firstly, a study using two different mouse models of colon cancer found that mice carrying a dominant negative *RhoA* transgene ($RhoA^{T19N}$) had increased tumor burden [64]. Secondly, another study demonstrated that the loss of RhoA exacerbates, rather than diminishes, the formation of oncogenic K-Ras-induced lung adenocarcinomas in mice [65]. Additionally, the *RHOA* gene is rarely amplified in human tumors and has been predicted to be deleted according to the TCGA data sets [66]. Moreover, deep sequencing technologies have identified not only gain-of-function but also loss-of-function mutations in the *RHOA* gene [67, 68], with some of these mutations driving the growth of different cancer types. These findings highlight the complexity of the RHOA GTPase pathways in many human tumors and the need for further investigation into the impact of these alterations on tumor development.

1.7.1. *RHOA* mutations in cancer

Although RAS and RAC1 share common hotspot residues, the mutational hotspots in *RHOA* are notably different and occur in functionally diverse regions of the protein. In cancer, the majority of *RHOA* alterations are found at Gly^{17} (44%), with the $RHOA^{G17V}$ mutant being the most prevalent (78%). Mutations at Tyr^{42} and Arg^{5} occur at much lower frequencies (7% each), followed by Cys^{16} and Glu^{40} (3% each). Missense *RHOA* mutations have been identified in several tumor types, including peripheral T-cell lymphomas (PTCL), stomach cancer, and B-cell lymphomas, among others [69].

Among PTCLs, *RHOA* mutations have the highest frequency, occurring in over 20% of cases (**Figure 7A**). Specifically, angioimmunoblastic T-cell lymphomas (AITL) have *RHOA* mutations in up to 50% of the cases, surpassing peripheral T-cell lymphomas not-otherwise specified (PTCL-NOS) and adult T-cell lymphoma/leukemia (ATLL) (**Figure 7B**). Notably, mutations in PTCLs primarily affect the GTP-binding domains, whereas mutations in other tumors are less common but more diverse, primarily affecting the switch domains (**Figure 7C**). The specific residues mutated in each tumor type are indicated in **Figure 7D**.

In this introduction, we present an overview of the well-characterized *RHOA* mutations and categorize them according to their influence on the activity of the protein. For a comprehensive compilation of all reported *RHOA* mutations in human tumors, please consult **Table 1**.

The first group of mutations involves the disruption in hydrolysis (**Figure 8B**). They are deficient in GTPase activity and, consequently, render the protein constitutively activated. Unlike RAS genes, the mutations are found at very low levels in specific tumor subtypes. They typically target codons like those found in classical RAS proteins, such as Gly^{14} and Gln^{63}. Among these mutations, $RHOA^{Q63K}$ has been identified in colorectal and bladder cancer, albeit at low frequencies [67]. There are two common RHOA mutations, $RHOA^{G14V}$ and $RHOA^{Q63L}$, which are deficient in GTPase activity and, consequently, render the protein constitutively activated. Although these mutations are in the GTP-binding domain of the protein, they show differences at the functional level. For instance, fibroblast shows altered morphology when expressing $RHOA^{Q63L}$, features that are not recapitulated when expressing $RHOA^{G14V}$ [70]. These mutants also show different

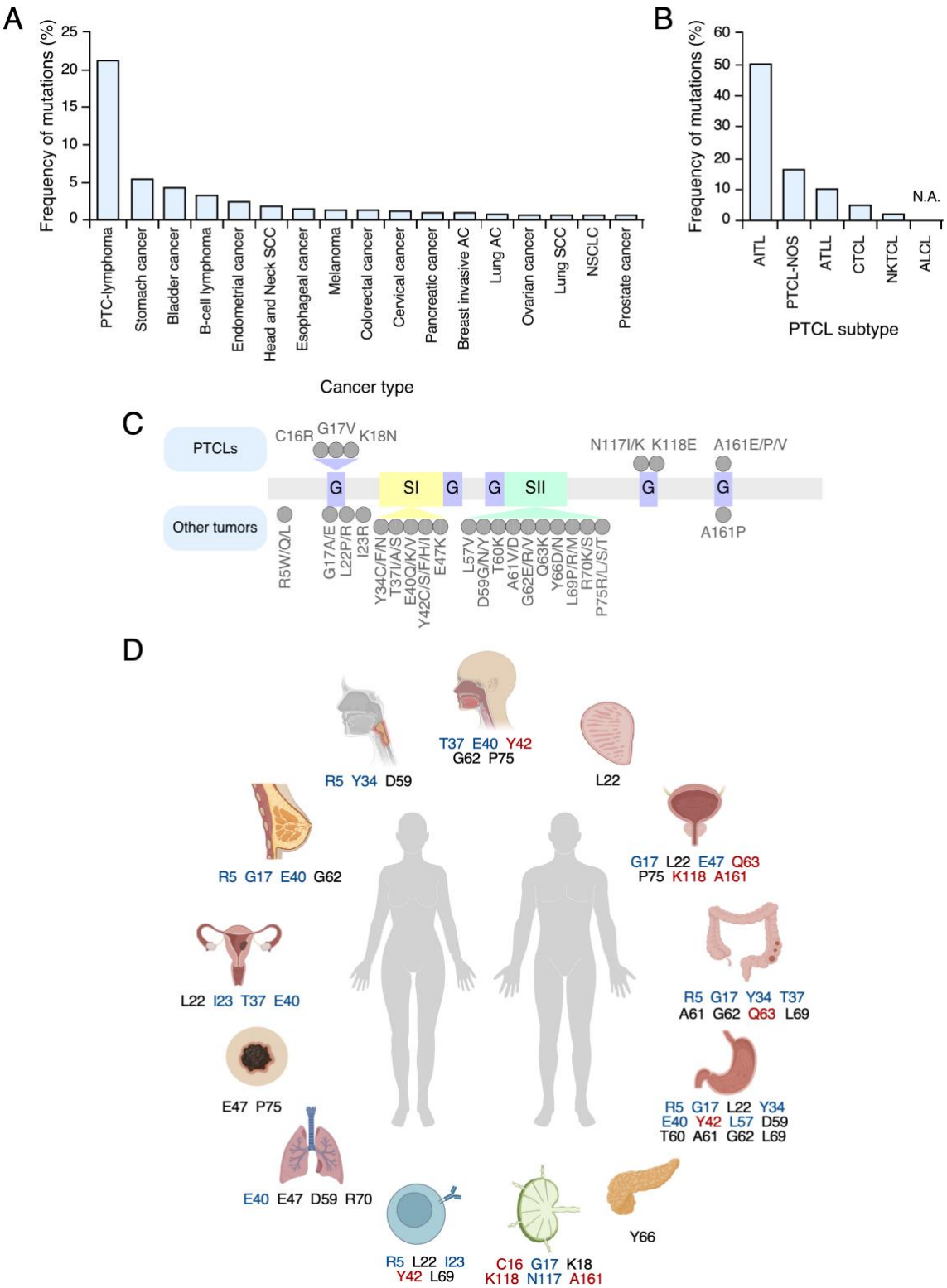

Figure 7. *RHOA* mutations found in human tumors. (A) Frequency of *RHOA* mutations in different tumor types. SCC: squamous cell carcinoma; AC: adenocarcinoma; NSCLC: non-small cell lung cancer. **(B)** Distribution of *RHOA* mutations in different subtypes of PTCL. AITL: angioimmunoblastic T cell lymphoma; PTCL-NOS: peripheral T cell lymphoma not otherwise specified; ATLL: adult T cell lymphoma/leukemia; CTCL: cutaneous T cell lymphoma; NKTCL: Natural Killer/T cell lymphoma; ALCL: anaplastic large cell lymphoma. N.A., not available. **(C)** Schematic representation of the distribution of *RHOA* mutations according to the tumor type. Mutations found in PTCLs are located at the top of the scheme, whereas the mutations found in other

tumors are depicted at the bottom. G: GTP-binding domain; SI: Switch I; SII: Switch II. **(D)** Example of main mutations found in *RHOA* gene in the indicated tumors. These mutations have been collected from information present in the cBioPortal (http://www.cbioportal.org), St. Jude Cloud PeCan (https://pecan.stjude.cloud/home), and recent publications on this topic. Red, gain-of-function mutation; blue, loss-of-function mutation; black, not characterized.

subcellular localization, being its ability to interact with RHOGDI altered [71]. One explanation to these findings is the fact that, although they produce similar changes in the switch I domain, they generate important differences in the switch II domain [72].

One mutation that has similar impact on the activity of the protein to the previous mentioned mutations, although some controversial studies contradict it, is the mutation of the residue Tyr^{42} (**Figure 8C**) This gene alteration has a high mutation rate within the switch I domain and is found mutated in diffuse-type gastric cancer [73, 74], head and neck squamous cell carcinoma [68], Burkitt's lymphoma, and diffuse large B-cell lymphomas [75, 76]. The most common mutation at this position is $RHOA^{Y42C}$. Initially, $RHOA^{Y42C}$ was considered a loss-of-function mutation using pulldown assays with Rhotekin, preventing anoikis in mouse intestinal organoids [74], and inactivating ROCK, thereby affecting cell survival and migration in gastric cancer cell lines [77]. However, subsequent reports indicated that $RHOA^{Y42C}$ is a gain-of-function mutation that may have growth-promoting advantages in diffuse-type gastric carcinoma [73]. Recently, these data have been corroborated as $RHOA^{Y42C}$ impairs intrinsic and GAP-stimulated GTP hydrolysis [78]. Furthermore, unlike the mutation at residue Gln^{63}, one intriguing aspect of this mutations is the interaction with certain effectors. While $RHOA^{Y42C}$ interacts with RHOGDI and mDia similarly to $RHOA^{WT}$, it exhibits a stronger interaction with ROCK and loses its interaction with Rhotekin [78] (**Figure 8C**).

Under normal conditions, the Tyr^{42} residue of RHOA undergoes phosphorylation by c-Met, promoting RHOA polyubiquitination and subsequent proteasome-mediated degradation. However, $RHOA^{Y42C}$ cannot be phosphorylated, resulting in its stability, and promoting proliferation, migration, and invasion of gastric cancer cells [18]. In line with this, mouse models have demonstrated the role of mutations in Tyr^{42} in cancer progression and tumorigenesis in gastric cancer. An orthotopic xenograft model expressing $RHOA^{Y42C}$ and $RHOA^{Y42S}$ presented a decrease in inflammation- and hypoxia-related pathways, but an enrichment in cell metabolism-, ROCK signaling inhibition-, and cell cycle-related pathways [79]. In addition, the expression of $RHOA^{Y42C}$ in combination

with *Cdh1* loss in mice produces a phenotype associated with transformation, resembling the morphologies of patient-derived diffuse-type gastric cancer organoids. This effect is mediated through the activation of ROCK, β-catenin and FAK, which further activated the PI3K/AKT and YAP/TAZ pathways [78].

Consequently, the role of the mutation *RHOA*^{Y42C} in tumorigenesis might not only be attributed to its gain-of-function mutation nature, but also to the alterations in its interaction with effector proteins and regulators, as well as its posttranscriptional modifications. In fact, these alterations could have a more dramatic effect on tumorigenesis than the hyperactivation of its intrinsic catalytic activity, the effects produced by these alterations are less predictable.

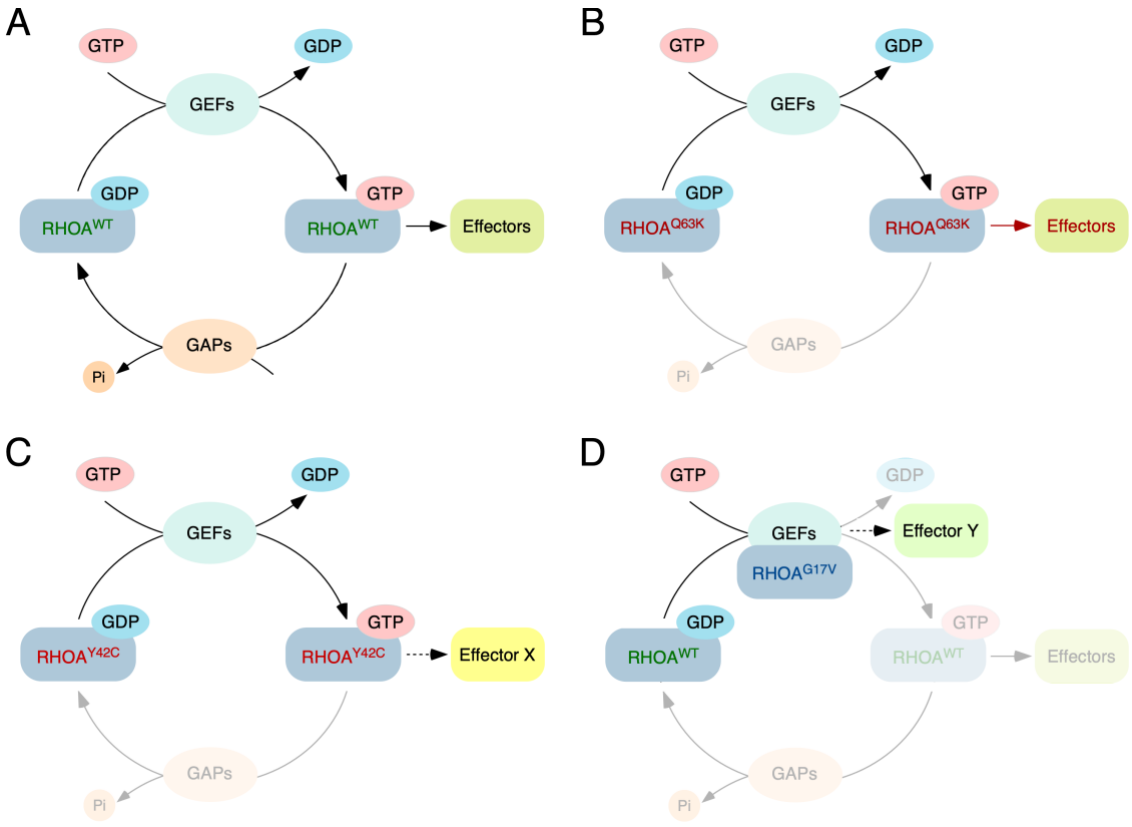

Figure 8. Consequences of mutations on RHOA GDP-GTP regulation and effector interaction. **(A)** RHOA activation cycle in unaltered conditions (RHOA^{WT}). **(B)** RHOA activation cycle of the constitutively active version RHOA^{Q63K}, which impairs intrinsic and GAP-stimulated GTP hydrolysis activity and enhances nucleotide exchange. **(C)** The RHOA^{Y42C} mutant disrupts GDP-GTP regulation and differentially alters effector interactions. It exhibits intrinsic and GAP-stimulated GTP hydrolysis. **(D)** The mutant protein RHOA^{G17V} results in a nucleotide-free mutant protein that acts as a dominant negative protein and forms non-productive complexes with RHOA-selective GEFs. This results in the blockage of the activation of wild type RHOA, as well as in novel functions. The shaded regions represent the level of activity or binding altered in each case.

In addition to these activating mutations, it is worth noting the presence of *RHOA* mutations that lead to the loss of protein function. One example of such mutations affects the Arg^{5} residue, being the most common mutants $RHOA^{R5Q}$ and $RHOA^{R5W}$. These mutations have been identified in Burkitt lymphoma and diffuse large B cell lymphoma, where the most common change is $RHOA^{R5Q}$ [75, 76, 80]. They also appear in diffuse-type gastric cancer [73, 74], colorectal cancer and esophageal cancer [68]. However, in these types of tumor the most prevalent mutation is $RHOA^{R5W}$. The activity of these mutants was evaluated using pull down and SRF-SR luciferase assays, demonstrating that both $RHOA^{R5Q}$ and $RHOA^{R5W}$ are loss-of-function mutations [75, 81]. The $RHOA^{R5Q}$ mutant has been reported to be involved in B-cell lymphomagenesis by altering the $G\alpha_{13}$/RhoA axis [75]. On the other hand, the $RHOA^{R5W}$ mutant was demonstrated to affect aggregation but not migration in a gastric cell line [81].

However, the most intriguing example of loss-of-function mutant in RHOA is the mutation affecting the Gly^{17} residue in the GTP-binding domain (**Figure 8D**). This mutation was initially discovered in angioimmunoblastic T-cell lymphomas (AITLs) [82] and PTCL-NOS [83], as well as in solid tumors such as diffuse-type gastric cancer [74]. Specifically, different studies found that about 70% of AITL cases and 8-18% of PTCL-NOS samples carry the same mutation at Gly^{17}, with $RHOA^{G17V}$ being the more prevalent substitution. This mutation is a loss-of-function mutation that leads to the sequestration of GEF proteins, thus inactivating the wild-type RHOA function [82, 84, 85]. This dominant negative function has been supported by the inhibition of serum response factor-responsive element (SRF-RE) reporter activity and the decrease in stress fiber formation [82, 83] (**Figure 8D**). However, it is noteworthy that many studies have reported that $RHOA^{G17V}$ mutant can act as driver in different subtypes of PTCL.

Interestingly, this mutation frequently co-occurs with mutations in *TET2* and *DNMT3A*, genes encoding proteins involved in epigenetic programming [82]. In line with this, the cooperation between *TET2* deficiency and *RHOA* in AITL lymphomagenesis has been investigated in different mouse models. *TET2* loss and $RHOA^{G17V}$ expression in mature murine T cells cause abnormal proliferation and differentiation of $CD4^{+}$ T cells by decreasing FoxO1 levels in the nucleus, leading to impaired $CD4^{+}$ T cell function and immune-inflammatory phenotypes in AITL [86]. Similar results have been observed in a murine model expressing $RhoA^{G17V}$ under the control of murine CD4 regulatory elements.

RhoA^{G17V} expression alone induced autoimmunity in mice, but in the absence of *Tet2*, the mice developed AITL characterized by the gene sets reflecting mTORc1 activity [87]. In another study, expression of *Rhoa*^{G17V} in CD4^{+} T cells induces T_{FH} differentiation towards an increase of T_{FH}-specific surface markers. Mice containing bone marrow progenitors from *Tet2* knockout mice expressing *RHOA*^{G17V} developed AITL, where ICOS signaling led to an increase in tumor proliferation by activating on the PI3K-mTOR signaling [88]. Collectively, these data demonstrate that the RHOA^{G17V} mutant alone is not sufficient to cause tumorigenesis, but cooperation between RHOA^{G17V} mutant and *TET2* loss is necessary for lymphomagenesis to occur.

Table 1. *RHOA* mutations described in human tumors (continues in next page).

Mutation	Localization	Tumor type	Type	References
R5Q	Other	Burkitt's lymphoma Diffuse large B- cell lymphoma Diffuse-type gastric cancer Colorectal cancer Esophageal cancer	LOF	[55, 58, 60, 66-70]
R5W	Other	Diffuse-type gastric cancer Colorectal cancer Esophageal cancer Burkitt's lymphoma Diffuse large B- cell lymphoma	LOF	[55, 58, 60, 66-70]
C16R	G box	Adult T-cell leukemia/lymphoma	GOF	[55, 63]
G17V	G box	Angioimmunoblastic T-cell lymphoma PTCL-NOS Adult T-cell leukemia/lymphoma	LOF	[55, 57, 59, 61-63]
G17A/E/R	G box	Breast cancer Diffuse-type gastric cancer Bladder cancer Adult T-cell leukemia/lymphoma	LOF	[55, 64]
L22P/R	G box	Stomach cancer Burkitt's lymphoma Prostate cancer Bladder cancer	Not characterized	[55, 60, 68]
I23R/L	Other	Burkitt's lymphoma Endometrial cancer	LOF	[68]
Y34C/F/N	Switch I	Colorectal adenocarcinoma Diffuse-type adenocarcinoma	LOF	[71, 72]
T37I/A/S	Swich I	Colorectal adenocarcinoma Head and neck squamous cell carcinoma	LOF	[71-73]
E40Q/K/V	Switch I	Breast cancer Diffuse-type gastric cancer Lung squamous cell cancinoma Head and neck squamous cell carcinoma	LOF	[71-73]

Table 1. *RHOA* mutations described in human tumors (continuation from previous page).

Mutation	Localization	Tumor type	Type	References
Y42C/S/F/H/I	Switch II	Diffuse-type gastric cancer Head and neck squamous cell carcinoma Burkitt's lymphoma Diffuse large B-cell lymphoma	GOF	[55, 60, 67-69, 74]
E47K	Switch II	Lung squamous cell carcinoma Bladder cancer	LOF	[55, 71]
L57V	Switch II	Diffuse-type gastric cancer	LOF	[60]
D59G/N/Y	Switch II	Stomach cancer Lung adenocarcinoma	Not characterized	[71]
T60K	Switch II	Stomach cancer	Not characterized	[71]
A61D/V	Switch II	Stomach cancer Colorectal adenocarcinoma	Not characterized	[71]
G62E/R/V	Switch II	Stomach cancer Colorectal adenocarcinoma Breast cancer Head and neck squamous cell carcinoma	Not characterized	[71]
Q63K	Switch II	Colorectal adenocarcinoma Bladder cancer	GOF	[71]
Y66D/N	Swicth II	Pancreatic cancer	Not characterized	[71]
L69P/R/M	Switch II	Colorectal adenocarcinoma Stomach cancer Burkitt's lymphoma	Not characterized	[68, 69, 71]
R70K/S	Switch II	Renal clear cell carcinoma Cutaneous melanoma	Not characterized	[71]
P75R/L/S/T	Switch II	Bladder cancer Head and neck squamous cell carcinoma	Not characterized	[71]
N117I/K	G box	Cutaneous T-cell lymphoma	LOF	[65]
K118E/N	G box	Adult T-cell leukemia/lymphoma	GOF	[63]
A161P/E/V/T	G box	Adult T-cell leukemia/lymphoma Bladder cancer	LOF (A161E) GOF (A161P)	[63, 71]

Other changes affecting the Gly^{17} residue of RHOA have been found in human tumors, such as *RHOA*^{G17E}, *RHOA*^{G17A}, or *RHOA*^{G17R}. These mutations are mainly found in solid tumors including breast cancer, diffuse-type gastric cancer, or bladder cancer, although they are also found in ATLL to a lesser extent [68]. Among these mutations, G17E is the most common and has been shown to be a loss-of-function mutation in different gastric cancer cell lines [77].

Of interest are the *RHOA* mutations reported in adult T-cell leukemia/lymphoma (ATLL), including *RHOA*^{G17V}, *RHOA*^{C16R}, *RHOA*^{A161E}, and *RHOA*^{A161P}, being the Cys^{16}

residue the most frequently affected. Surprisingly, depending on the positions and the type of mutation, these RHOA mutants display different and opposing biological functions in terms of activation status, transcriptional activation, or regulation of stress fibers, with $RHOA^{G17V}$ and $RHOA^{A161E}$ being loss-of-function mutants and $RHOA^{C16R}$ and $RHOA^{A161P}$ being gain-of-function mutants [89].

In summary, at present, only a limited number of *RHOA* mutations found in tumors have been characterized, while many other mutations remain unstudied, with their effects yet to be determined. Specifically, when considering mutations associated with PTCLs, the presence of dominant negative mutants according to the established functional archetypes, along with mutants displaying GOF properties, has further complicated our understanding of the role of RHOA in cancer. This counterintuitive observation requires further investigation, with a specific focus on unraveling the signaling mechanisms responsible for triggering tumorigenesis in the presence of these specific mutations. Therefore, we have decided to focus our work on investigating the actual contribution of *RHOA* mutations in cancer, with a particular emphasis on mutations associated with PTCL.

2. PERIPHERAL T-CELL LYMPHOMAS

2.1. T LYMPHOCYTES

T cells are a subset of white blood cells responsible for the adaptive immune response. They originate from bone marrow progenitors and undergo a process of maturation in the thymus, which is the primary site of T cell development. In the thymus, bone marrow progenitors lacking $CD4^+$ and $CD8^+$ coreceptors undergo T cell receptor (TCR) rearrangement to generate $CD4^+CD8^+$ double-positive thymocytes. These double-positive cells are then rigorously selected through the interaction with thymic epithelial cells and thymic dendritic cells, giving rise to $CD4^+$ or $CD8^+$ single-positive thymocytes, which finally exit the thymus as naïve T cells. There are two main types of T-cells: cytotoxic T cells, which are $CD8^+$, and helper T cells, which are $CD4^+$. Cytotoxic T cells kill cells infected with bacteria, viruses, or even cancer cells, whereas helper T cells send signals to other immune cells to coordinate an attack against an aggressor. Once fully maturated, T cells travel to tissue and organs of the lymph system, such as the spleen, lymph nodes and tonsils, or circulate in the bloodstream [90].

In the context of $CD4^+$ T cells, the circulating T cell population can be divided in three different subsets: naïve T cells, memory T cells, and regulatory T cells. Naïve T cells are able to respond to new antigens, while memory T cells maintain long-term immunity and regulatory T cells control the immune responses. The differentiation of naïve T cells to memory or effector/helper T (T_H) cells begins when they recognize specific antigens presented by antigen-presenting cells (APCs) through their TCR. Each helper T cell subset has a characteristic expression of surface markers, transcription factors, growth factor, chemokines, and chemokine receptors, which contribute to their specialized functions and adequate T cell response. These T helper cells include: Th1 cells, characterized by the expression of the transcription factor TBX21 and production of significant amounts of IFN-γ; Th2 cells, expressing GATA-3 and secreting IL-4, IL-5, and IL-13; Th17 cells, which express ROR-γt and produce IL-17A, IL-17F, and IL-22; regulatory T cells (Treg), which express Foxp3 and produce TGF-β; and T follicular helper (T_{FH}) cells, identified by the expression of BCL6 and secretion of IL-21 [91]. Effector T cells possess long-term survival capabilities and can reside in secondary lymphoid organs or infected tissues [92].

2.2. T CELL RECEPTOR COMPLEX

The TCR is a multiprotein complex that is responsible for antigen recognition in T cells (**Figure 9**). It consists of two subunits, αβ or γδ, each with an extracellular region, a transmembrane region, and a short cytoplasmic tail. The extracellular region contains a variable immunoglobulin-like (V) domain and a constant immunoglobulin-like (C) domain along with a linker peptide. The C domain is used for the interactions with CD3 chains (CD3ε, CD3ζ, CD3δ, and CD3γ), which are necessary for initiating the signaling when the TCR recognizes an antigen. Moreover, the TCR complex contains ten immunoreceptor tyrosine-based activation motifs (ITAM) in the cytoplasmic tail of the CD3 molecules, which consist of tandem duplications of a sequence containing a tyrosine (YXXXL/I) (**Figure 9**). One of these motifs is present in the CD3γ/ε/δ chains and three of them in the CD3ζ chains [93, 94].

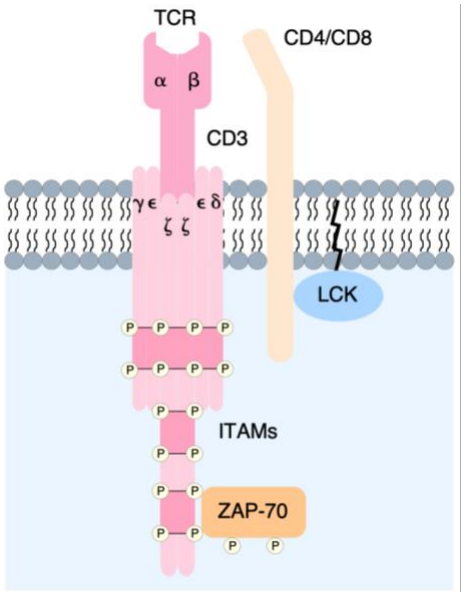

Figure 9. TCR complex. TCRα and TCRβ heterodimers form complexes with CD3εγ, CD3εδ and a homodimer CD3ζζ. The co-receptors CD4 or CD8 are also indicated, as well as the ITAM motifs, and the protein kinases LCK and ZAP-70.

T cells also have CD4 and CD8 co-receptors that consist of an extracellular domain, a transmembrane domain, and a short intracellular domain (**Figure 9**). The extracellular domain of CD4 contains two V domains and two C domains, acting as a monomer on the T cell surface. In contrast, the extracellular domain of CD8 consists of one V domain. Another important difference between CD4 and CD8 co-receptors is the

type of ligand that they recognize. $CD8^+$ T cells recognize antigen peptide-bound major histocompatibility complex (MHC) type I, which can be found in any antigen presenting cell recognized by $CD8^+$ T cells. In contrast, $CD4^+$ T cells recognize MHC type II molecules, which are presented by the antigen-presenting cells (APCs), such as macrophages, dendritic cells, or B cells [95].

In addition to its main components, the TCR complex also comprises different protein tyrosine kinases belonging to the SRC family, such as LCK or FYN, as well as kinases of the SYK family such as ZAP-70 [94] (**Figure 9**).

2.3. T CELL RECEPTOR SIGNALING

Early T cell signaling takes place within seconds upon antigen binding to the extracellular domain of the TCR. This process involves the phosphorylation of tyrosine residues by protein tyrosine kinases (PTKs), which generate docking sites for signaling molecules with phosphotyrosine recognition domains that initiate proximal signals [95].

Upon recognition of an antigen by the TCR, LCK interacts with the co-receptors CD4 or CD8, which bind to the TCR. This facilitates the recognition of the antigen by the TCR and promotes the autophosphorylation of LCK which, in turn, leads to the phosphorylation of ITAMs by LCK [96]. This phosphorylation allows the recruitment and binding of ZAP-70, which becomes activated (**Figure 10**).

When activated, ZAP-70 phosphorylates LAT on different tyrosine residues. LAT acts as a central hub for recruiting various signaling molecules (**Figure 10**). For example, GRB2 and GADS are cytosolic proteins that translocate to the plasma membrane upon binding to phosphorylated LAT. GRB2 is constitutively associated with SOS and activates RAS signaling [95]. Activated GADS binds SLP76, leading to PLCγ1 activation [97]. SLP76 also serves as a binding site for proteins such as the nucleotide exchange factor VAV1, NCK, ITK, and ADAP [95, 97, 98]. The activation of VAV1 promotes RAC1 activation which, in turn, stimulates the ARP2/3 complex, ensuring actin polymerization and branching [99]. Furthermore, RAC1 signaling is activated in response to stress stimuli, leading to the activation of JNK/p38 pathway [100] (**Figure 10**).

Active PLCγ1 catalyzes the cleavage of PIP_2 to obtain the second messenger diacylglycerol (DAG) and inositol trisphosphate (IP_3) (**Figure 10**). In the plasma membrane, DAG activates proteins such PKCθ and RASGRP1. PKCθ activates the AP-1 transcription factor through the phosphorylation and activation of the kinase SPAK, and forms a complex with CARD11, BCL10, and MALT1 that will allow the translocation of the NFκB transcription factor to the nucleus. Meanwhile, RASGRP1, together with SOS, activates the RAS/MAPK cascade inducing the activation of the AP-1 transcription factor [94, 95, 101]. Moreover, VAV1 and PLCγ1 also stimulate and activate RASGRP1, which, in turn, activates RAS/MAPK signaling pathway [94] (**Figure 10**).

IP_3 diffuses through the cytoplasm and binds to the Ca^{2+}-permeable ion channel receptors (IP3R) on the endoplasmic reticulum (ER). This binding results in the release of calcium from the ER stores and the influx of extracellular calcium through channels in the plasma membrane, such as ORAI1 [102]. The increased intracellular Ca^{2+} then activates the phosphatase calcineurin, which dephosphorylates the nuclear factor of activated T cells (NFAT) family of transcription factors, leading to their translocation to the nucleus. There, NFAT activates the expression of genes related to T cell activation, proliferation, and differentiation. Additionally, Ca^{2+} activates Ca^{2+}/calmodulin-dependent kinase (CaMK), which is implicated in the activation of transcription factors such as myocyte enhancer factor (MEF2) and cyclic-AMP-responsive-element-binding protein (CREB) [94, 95, 103, 104] (**Figure 10**).

In addition to LCK, PI3K is also activated by the TCR and the costimulatory molecule CD28 (**Figure 10**). This enzyme phosphorylates PIP_2 to obtain phosphatidylinositol (3, 4, 5)-trisphosphate (PIP_3), recruiting proteins to the plasma membrane such as ITK. Once active, ITK phosphorylates and activates PLCγ1 [105]. Apart from ITK, PIP_3 also recruits PDK1, which is responsible for the activation of AKT. Active AKT inactivates GSK3, which maintains NFAT activity in the nucleus, and recruits CARD11, favoring the activation of the NF-κB pathway. Furthermore, AKT induces the activation of mTOR, which promotes STAT3 activity to promote Th17 differentiation [95] (**Figure 10**).

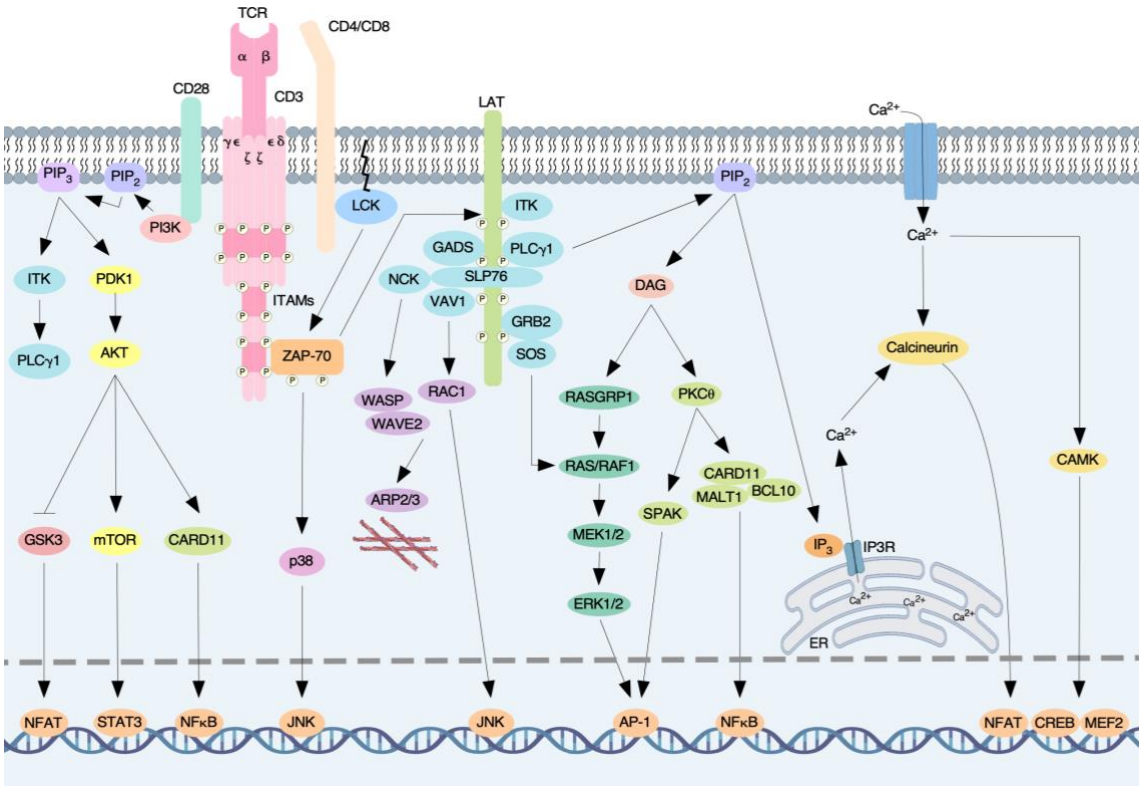

Figure 10. Main TCR signaling pathways. Upon TCR activation the kinase LCK binds to the cytoplasmic domain of the CD4 and CD8 co-receptor and is recruited to the TCR, where it phosphorylates and activates ITAMs in the CD3 chains, enabling the activation of ZAP-70. ZAP-70 phosphorylates LAT, promoting the recruitment and activation of several adaptor and effector molecules. Activation of LAT-associated effector proteins results in the activation of different transcription factors, including NFAT, NF-κB, AP-1, JNK, CREB, MEF2, and STAT3.

2.4. PERIPHERAL T-CELL LYMPHOMAS

Peripheral T-cell lymphomas is a group of rare and highly heterogeneous malignancies that arise from mature T and NK cells. They constitute approximately 10-15% of all non-Hodgkin lymphomas in Western countries, and around 20-30% in Asia and South America [106, 107]. The heterogeneity of PTCLs is reflected in the last World Health Organization classification of lymphoid neoplasms, which recognizes more than 30 subtypes [108]. These subtypes include nodal, extranodal, cutaneous and leukemic forms. The most common disorder is PTCL not otherwise specified (PTCL-NOS), comprising approximately 30% of PTCLs. Other subtypes include angioimmunoblastic T cell lymphoma (AITL), anaplastic large cell lymphoma (ALCL), and extranodal natural killer cell/T cell lymphoma (ENKTCL), which account for 10-30%, 15%, and 5-6% of cases, respectively. Notably, some PTCLs are geographically localized, and others are driven by viral infections [109].

The classification of PTCL has undergone major changes over the past years considering the notion that PTCL can arise from different subsets of normal T cells. This information (see T lymphocytes section) reveals that a substantial proportion of PTCL-NOS cases are related to either Th1 or Th2 lineage derivation. Specifically, PTCL-NOS TBX21^{+} is derived from Th1 cells, while PTCL-NOS positive for the transcription factor GATA3 is derived from Th2 cells. The T_{FH} cell subset represents the cell of origin of follicular T cell lymphoma, AITL, and nodal PTCL with T_{FH} cell phenotype, whereas Treg cells are considered the precursors of adult T cell leukemia/lymphoma and Sezary Syndrome. Cutaneous T cell lymphomas arise from CD4^{+} T cells specialized in homing to the skin, whereas ALCL derives from Th17 cells [109] (**Figure 11**).

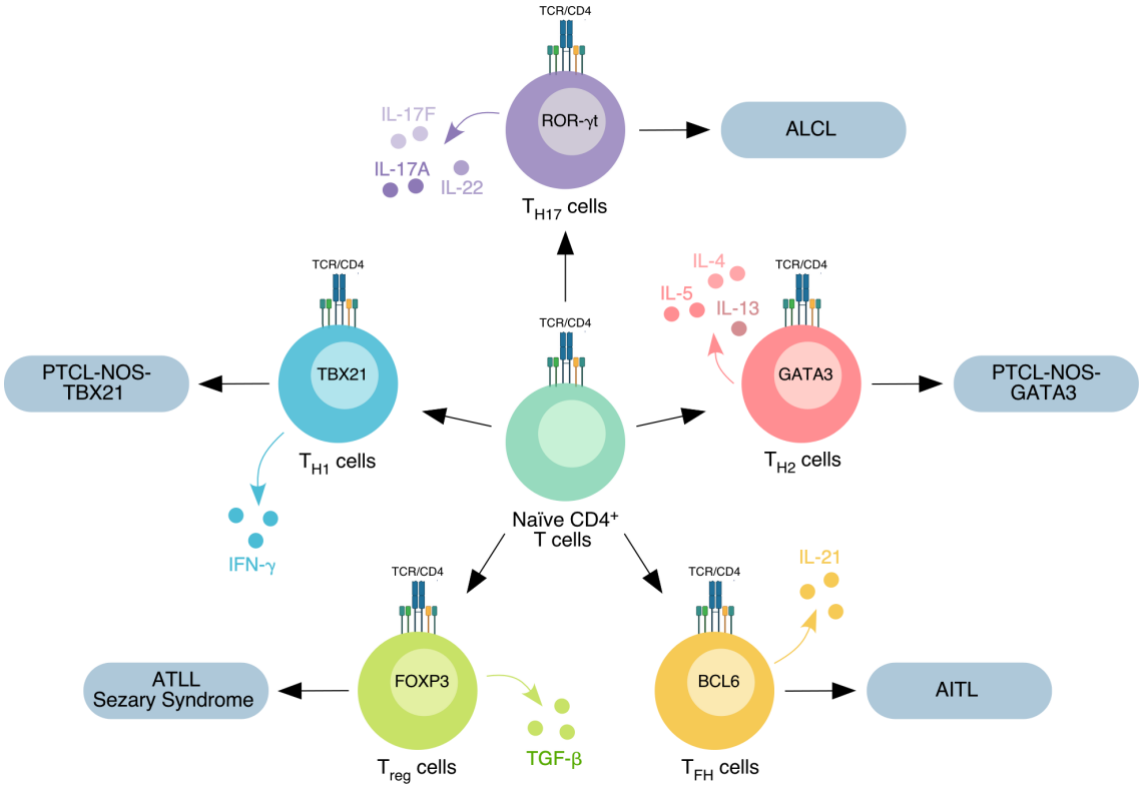

Figure 11. T helper cell lineages and their connection with PTCL development. Naïve CD4^{+} T cells differentiate into distinct T helper subsets, each characterized by a specific transcription factor and cytokine secretion profile. The PTCL subtypes indicated arise from these specific T helper cell lineages, representing their cell of origin.

2.4.1. Pathogenesis

The pathogenesis of PTCL comprises different mechanisms, including the deregulation of signaling pathways, recurrent genomic and epigenomic alterations, and virus-mediated

transformation [109]. For example, PTCL-NOS is characterized by increased transcription of genes such as *MYC*, *STAT3*, or *CDK6* [110], whereas GATA3-PTCL-NOS is associated with by the loss of *CDKN2A*, *RB1*, *TP53*, *PTEN*, and other genetic alterations [111]. Recurrent translocations have also been described [109, 112].

Recent advances in next-generation sequencing have led to the discovery of recurrent mutations in genes involved in TCR signaling in PTCL, including missense mutations in *PLCG1*, *CD28*, *VAV1*, *FYN*, *RHOA*, or *KRAS* [113-118], as well as gene fusions affecting *ITK* (*ITK-SYK* and *ITK-FER)* [119, 120], *VAV1* (*VAV1-MYO1F*, *VAV1-THAP4* and *VAV1-S100A7)* [121, 122], and *CD28* (*CTLA4-CD28* and *ICOS-CD28)* [115, 123], among others. The JAK-STAT pathway is also deregulated in PTCL, AITL, and ALCL, mainly due to activating mutations in genes such as *JAK1*, *STAT3*, and *STAT5*, as well as inactivating mutations, abnormal gene methylation, and virus-mediated inhibition of the negative regulators *PTPN1* and *PTPN6* [109, 124]. Deregulation of the AP-1 signaling pathway due to amplifications and constitutive activation of *JUNB [125]*, as well as hyperactivation of the PI3K signaling as a consequence of mutations, amplifications, or overexpression of the PI3K-related genes *PIK3R1*, *PIK3R5*, *PIK3CA*, *PDPK1*, or *CTNNB1* are also common features of PTCLs [113].

Epigenomic alterations involving mutations in the genes encoding Ten-Eleven Translocation-2 (*TET2*), isocitrate dehydrogenase 2 (*IDH2*) and DNA methyltransferase 3A (*DNMT3A*) are also commonly found in PTCL, including Sezary Syndrome [126], AITL [83, 127], or PTCL-NOS [83], among others. These alterations mainly include the loss of *TET2* [128] or the mutation $IDH2^{R172}$ [129, 130].

Finally, certain PTCL subtypes have been associated with viral infections [109]. Specifically, Epstein-Barr virus (EBV) infects T or NK cells, producing certain mutations that cause the uncontrolled proliferation of these cells, leading to the development of lymphomas. PTCL-NOS and AITL EBV^{+} patients have decreased overall survival rate [131]. Additionally, ATLL is associated with human T cell lymphotropic virus type 1 (HTLV-1), which leads to the activation of AP-1 or NF-κB signaling pathways [132], and the deregulation of tumor suppressors (p53, RB, CDKs, etc.) [133].

From a clinical point of view, targeting the pathogenic mechanisms holds promise for therapeutic interventions in PTCLs. This disease is associated with poor prognosis,

with median overall survival rates of 1-3 years lower than 50%, except for ALK^+ anaplastic T-cell lymphoma, which exhibits a five-year survival of 80% [107, 134]. Unfortunately, there has been limited progress in improving survival rates for PTCL over the past three decades.

2.5. ANGIOIMMUNOBLASTIC T CELL LYMPHOMA

For the purpose of this thesis, a deeper description of the PTCL subtype called AITL is required. As previously mentioned, AITL is the second most prevalent subtype of PTCL, comprising 15-30% of non-cutaneous mature T and NK cell lymphomas. It exhibits varying geographical incidence, with Europe having the highest frequency (29%), followed by Asia (18%) and the USA (16%) [135]. This pathology develops late in life, with a median age of onset at 69 years, and most patients being diagnosed at an advance-stage of the disease (up to 80%). Consequently, the overall survival rate is poor, with a median survival of 5 years and only 32% of patients surviving past that period [135, 136].

2.5.1. Clinical presentation and pathogenesis

Patients with AITL typically present hepatosplenomegaly, diffuse lymphadenopathy, skin rashes, arthritis, ascites, and pleural effusion. Extranodal involvement is usually seen in the liver, skin, spleen, and bone marrow. Additionally, patients with AITL frequently suffer EBV infection, immune dysfunction, and immunodeficiency. Laboratory studies may also reveal Coombs-positive hemolytic anemia, elevated LDH, polyclonal hypergammaglobulinemia, cold agglutinins, or anti-smooth muscle antibodies [137].

Lymph nodes in AITL show effacement of the architecture with proliferation of endothelial venules and expanded follicular dendritic cell meshworks. The neoplastic T cells express T_{FH} markers such as PD1, ICOS, CXCR5, BCL6, CD10, CXCL13, and SAP. This specific subset of cells has been postulated to be the cell of origin of AITL [109]. Moreover, EBV-infected B cells are frequently found in the tumor microenvironment [138, 139].

T_{FH} cells are $CD4^+$ T cells located within the germinal center, where they play a crucial role in germinal center formation, B cell affinity maturation, and the development

of high-affinity antibodies and memory B cells [140]. Hence, these cells are central players in autoimmune features and B-cell proliferation in AITL tissue, in which tumor microenvironment supposes up to 90% of it [136]. In AITLs, tumoral T_{FH} cells release cytokines and chemokines to recruit immune cells into the tumor, including $CD4^+$ and $CD8^+$ T cells, B cells, macrophages, eosinophils, and dendritic cells. T_{FH} cells secrete CXCL13, a chemokine that binds to the receptor CXCR5, promoting the recruitment of B cells and dendritic cells and their subsequent activation, as well as the localization of T_{FH} cells into de germinal center. T_{FH} cells also release IL-21, a soluble factor that has an autocrine effect on T_{FH} cells, and IL-4, which contributes to B cell proliferation in the germinal center together with IL-21. Moreover, mast cells, dendritic cells and T_{FH} cells produce VEGF, a cytokine that recruits endothelial cells for the formation of new vessels in the tumor (**Figure 12**) [136, 141]. These mechanisms contribute to the origin of AITL features, such as the deregulated immune and inflammatory response, B-cell expansion, hypergammaglobulinemia, arborizing venules, or polymorphic cellular infiltrate.

2.5.2. Mutational landscape of angioimmunoblastic T-cell lymphomas

AITL is characterized by lower genomic complexity than other PTCL subtypes. Co-occurring gains of chromosomes 5 (43%) and 21 (23%) are frequently observed in AITL, which are significantly associated with the mutation $IDH2^{R172}$. In contrast, gain of chromosomes 7/7q, 11, 19, or 22q occurred in less than 10% of the cases. The chromosome 5 gain is associated with upregulation of several genes, including *IL4*, *IL13*, *MAPK9*, as well as genes related to T-cell activation and cell cycle. Moreover, focal deletions were observed in specific loci in non-mutated *IDH2* samples, showing enrichment of genes regulating negatively PI3K-AKT-mTOR and NF-κB pathways [111].

Next-generation sequencing has led to the discovery of recurrent mutations in AITL. The most frequent mutations affect the epigenetic modifiers *TET2*, *DNMT3A*, and *IDH2*, as well as *RHOA*, which frequently co-occur [82, 83, 130]. *TET2* inactivating mutations appear in up to 80% of cases, promoting DNA hypermethylation and abnormal regulation of gene expression. *DNMT3A* encodes a DNA methyltransferase mutated in 20-40% of cases, frequently in combination with *TET2* mutations. IDH2, a mitochondrial enzyme that transforms isocitrate to α-ketoglutarate, is mutated in around 30% of the

cases, almost exclusively at the R172 position, resulting in a novel enzymatic activity. In the case of *RHOA*, it is mutated in 50-70% of cases, with the G17V mutation being the most prevalent mutation. This mutation exclusively co-occurs with *TET2* mutations, with or without *IDH2* mutations. Moreover, the dual loss of *TET2* and *DNMT3A* has been found in AITL [142].

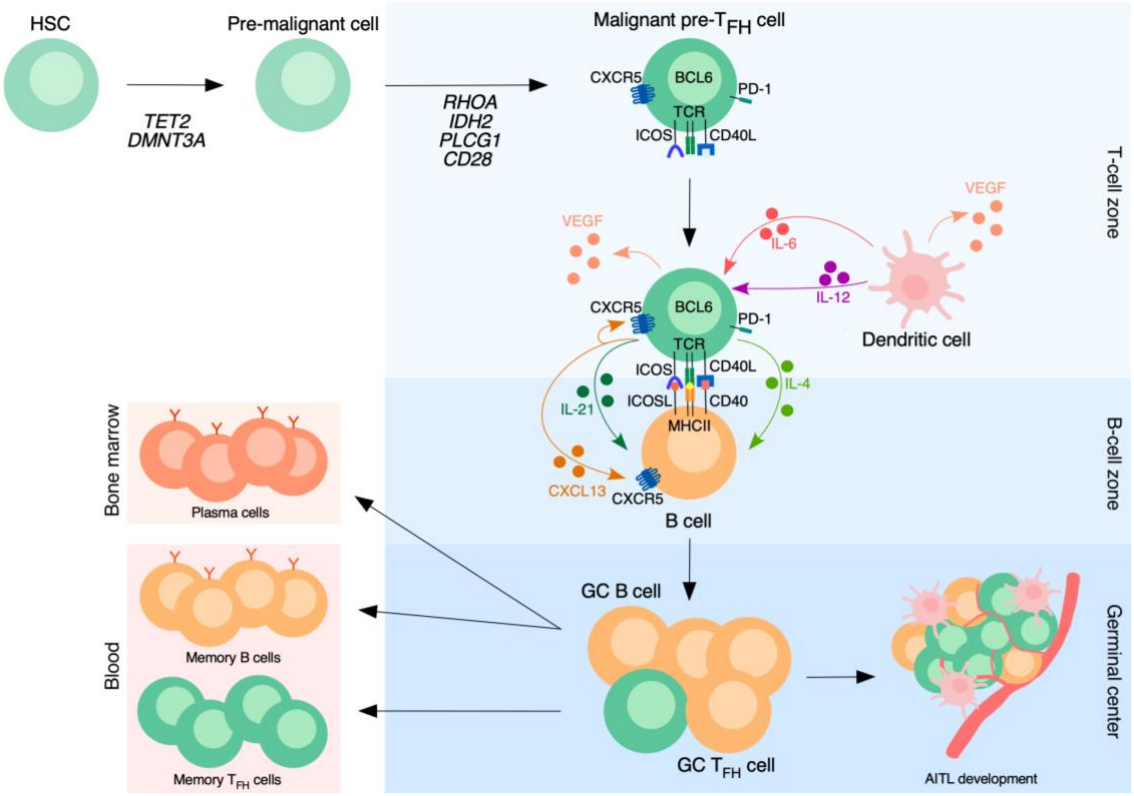

Figure 12. Schematic representation of AITL development. Early and successive oncogenic events synergize to produce AITL. First, the loss of epigenetic regulators (*TET2* or *DNMT3A*) in hematopoietic stem cells (HSC) generates pre-malignant cells. Subsequently, TCR-hyperactivating mutations (e.g., *RHOA*, *IDH2*, *PLCG1*, *CD28*) occur, leading to the differentiation of $CD4^+$ T cells into T_{FH} cells in the follicle. Aberrant activation and proliferation of T_{FH} cells contribute to AITL development. The AITL tissue is composed mainly by T_{FH} cells, which interact extensively with the tumor microenvironment, including B cells, dendritic cells, and endothelial cells. GC, germinal center; VEGF, vascular endothelial growth factor; BCL6, B cell lymphoma 6.

Furthermore, AITL patients show mutations in components of the TCR signaling pathway, including gene mutations in *PLCG1*, *CD28*, *VAV1*, and *FYN*, or gene fusions affecting genes such as *VAV1*, *CD28*, *CTLA4*, *ICOS*, *CARD11*, *CTNNB1*, *GTF2I*, and *PI3K*. CD28, a co-stimulatory molecule, is mutated in 10% of AITL cases, whereas the *CTLA4-CD28* gene fusion appears in up to 60% of cases. *FYN* mutations are rare, as is

the gene fusion *ITK-SYK*. Mutations in *PLCG1* and *CARD11* have been reported in 14% and 4% of AITL patients, respectively, leading to the hyperactivation of the NFAT and NF-κB pathways. PI3K signaling is increased in the cases in which mutations in the regulatory subunits PIK3R1 and PIK3R5 of PI3K are found, normally at low frequencies, or in AITL cases harboring mutations in *PDK1* or *CTNNB1* (6%). Finally, MAPK pathway hyperactivation has been reported in 6% of AITL cases harboring mutations in *GTF2I*, while *KRAS* and *STAT3* mutations are rare in AITL [83, 113, 114, 143].

AITL is thought to develop through a multistep tumorigenesis process (**Figure 12**). The first step involves somatic mutations in epigenetic regulators (*TET2*, *DNMT3A*), which occur in hematopoietic stem cells. These mutations lead to a pre-malignant state in the stem cells. Subsequently, naïve $CD4^+$ T cells mature to T_{FH} cells and experience a secondary mutation in TCR signaling pathways (*RHOA*, *VAV1*, *PLCG1*, or *CD28*). Finally, the interaction of the mature and mutated T_{FH} cells with various tumor immune microenvironment components results in the uncontrolled expansion of tumoral cells and ultimately leads to the development of AITL [82, 144, 145].

2.5.3. Treatment

At present, first-line treatment is based on chemotherapeutic agents such as CHOP, a combination of cyclophosphamide, doxorubicin, vincristine, and prednisone. Nevertheless, relapse rates are high, with approximately 80% in 5 years. Consequently, other alternatives, including the combination of CHOP with etoposide (CHOEP regimen), dose-adjusted etoposide, prednisone, vincristine, cyclophosphamide, and doxorubicin (DA-EPOCH), cyclophosphamide, dexamethasone/methotrexate, vincristine, doxorubicin, cytarabine (HyperCVAD), and Mega-CHOEP have been investigated, but they do not appear to provide any significant benefit compared to CHOP/CHOEP. Another first-line option is an aggressive approach that combines chemotherapy followed often by autologous stem-cell transplantation (ASCT) [146].

Various immunotherapies have been combined with CHOP, including monoclonal antibodies targeting the tumor microenvironment such as bevacizumab (anti-VEGF) or rituximab (anti-CD20), and the immunoregulator lenalidomide. However, their outcomes were similar to CHOP alone. A more promising first-line treatment for CD30-

positive AITL patients is the combination of brentuximab vedotin, an anti-CD30 drug conjugate, with cyclophosphamide, doxorubicin, and prednisone, which has been associated with improved outcomes [147].

As AITL undergoes important epigenetic changes during the oncogenic transformation process, different epigenetic-targeting drugs have been proposed, including histone deacetylase inhibitors (belinostat, vorinostat, or romidepsin) and hypomethylating agents such as 5-azacytidine. Histone deacetylase inhibitors have been approved for the treatment of refractory AITLs, with a response rate around 30%. In contrast, 5-azacytidine showed very promising results in relapsed/refractory AITL [109, 147, 148].

Targeted therapies are also directed towards specific signaling pathways. For instance, duvelisib, a PI3K inhibitor, and dasatinib, a multi-kinase inhibitor of TCR signaling, have resulted in partial responses in relapsed/refractory patients, with a response rate of approximately 50%. Furthermore, inhibitors of the JAK/STAT pathway, such as cerdulatinib or ruxolitinib, are currently under study [136, 148].

In summary, the lack of effective treatments for AITL, as well as other PTCL, highlights the need for further research in the discovery of new vulnerabilities that could lead to the development of new therapeutic options. The observed deregulation in epigenetic and T-cell signaling suggest that targeting these aberrant pathways in combination may be a promising strategy not only for AITL, but also for other PTCLs.

OBJECTIVES

The objectives of this Ph.D. thesis were:

1. To characterize the *RHOA* mutations described in human tumors.

2. To understand the mechanistic and pathobiological programs triggered by *RHOA* mutations in peripheral T-cell lymphomas.

3. To get new therapeutic insights into the treatment of $RHOA^{G17V}$-driven peripheral T-cell lymphomas.

METHODS

PLASMIDS

All the RHOA family constructs used in this work encode the human version of the protein. To generate the vectors encoding for the different RHOA mutants, site-directed mutagenesis was performed over the plasmids expressing human EGFP-tagged $RHOA^{WT}$ (pNM31) and AU5-tagged $RHOA^{WT}$ (pCEFL-AU5 $RHOA^{WT}$) using the high-fidelity NZYProof DNA Polymerase (Cat. #14601, NZYTech) and the primers listed in **Table 2**.

To generate retroviral vectors encoding HA-tagged RHOA mutants contained in the pMIEG3 vector (obtained from Yi Zheng, Cincinnati Children's Hospital, Cincinnati, OH) for the generation of Jurkat stable cell lines for proteomic analyses, the HA-tagged $RHOA^{WT}$ plasmid (pMCL20) was used as a template to carry out site-directed mutagenesis using the high-fidelity NZYProof DNA Polymerase and the correspondent primers listed in **Table 2**. To generate retroviral vectors encoding AU5-tagged RHOA mutants for the viral transduction of primary mouse $CD4^+$ T cells, the *RHOA* cDNA was amplified by PCR using the pCEFL-AU5 RHOA WT plasmid as a template, digested with EcoRI and XhoI, and ligated into the pMIG-II vector (Cat. No. 52107, Addgene) and the pMSCV-IRES-mCherry FP vector (Cat. No. 52114, Addgene). The primers used were: 5'- CTG ACA GAA TTC GCC GCC ACC ATG GGA TCC ACC GAC TTC TAC CTA AAG-3' (forward, EcoRI site underlined) and 5' – CTG ACA CTC GAG GCG TCA CAA GAC AAG GCA CCC AGA TTT TTT C – 3' (reverse, XhoI site underlined). The DNA sequence of all the generated plasmids were analyzed at the CIC Genomics Unit to confirm the presence of the desired mutations and absence of undesired ones. Then, these two new plasmids were used as a template to generate the desired *RHOA* mutations by performing site-directed mutagenesis using the Phusion High-Fidelity DNA Polymerase (Cat. No. F-530S, Thermo Scientific) and the corresponding oligonucleotide primers listed in **Table 2**.

The pSRF-luc and pAP1-luc plasmids were obtained from Stratagene (Cat. number 219081 and Cat. number 219087, respectively), the pNFAT-luc plasmid from Addgene (Cat. No. 17817), and the pRL-SV40 plasmid from Promega (Cat. number E2231), The pHes1-luc plasmid was kindly gifted by Anna Bigas (Institut Hospital del Mar d'Investigacions Mèdiques, Barcelona, Spain), whereas the pNF-κB-luc plasmid and pSTAT3-luc plasmid were generously gifted by Nancy C. Reich (Stony Brook University, New York, USA). The pCL-Eco and pPAX2 plasmids were obtained from

Addgene (Cat. number 12371 and Cat. number 12260, respectively), and the plasmids pMD-G and pNGVL-MLV-gag-pol were provided by Drs. R.C. Mulligan (Children's Hospital, Boston, MA, USA) and A. Bernard (CNIC, Madrid, Spain, EU), respectively.

Plasmids encoding human versions of the two isoforms of RAP1GDS1 HA-tagged (RAP1GDS1-558-HA and RAP1GDS1-607-HA) in a pcDNA3.1 plasmid were a gift from Carol L. Williams (Medical College of Wisconsin, Milwaukee, USA). Plasmids encoding the AU5-tagged human versions of CDC42 (pCEFL-AU5 CDC42 WT and pCEFL-AU5 CDC42 T17N), and RAC1 (pCEFL-AU5 RAC1 WT and pCEFL-AU5 RAC1 T17N) were kindly gifted by Piero Crespo (IBBTEC, Santander, Spain). The GFP-tagged version of these proteins was generated by Nieves Movilla.

Table 2. Primers used for the generation of *RHOA* mutations by site-directed mutagenesis (continues in next pages).

RHOA mutation	Primer sequence (5'→3')	
R5W	Forward	CCACCGATGGCTGCCATCTGGAAGAAACTGGTGATTG
	Reverse	CAATCACCAGTTTCTTCCAGATGGCAGCCATCGGTGG
C16R	Forward	GTGATTGTTGGTGATGGAGCCCGTGGAAAGACATGCTTGCTCATA
	Reverse	TATGAGCAAGCATGTCTTTCCACGGGCTCCATCACCAACAATCAC
G17A	Forward	GACTATGAGCAAGCATGTCTTTGCACAGGCTCCATCACCAACAATC
	Reverse	GATTGTTGGTGATGGAGCCTGTGCAAAGACATGCTTGCTCATAGTC
G17E	Forward	GACTATGAGCAAGCATGTCTTTTCACAGGCTCCATCACCAACAATC
	Reverse	GATTGTTGGTGATGGAGCCTGTGAAAAGACATGCTTGCTCATAGTC
G17V	Forward	GTGATTGTTGGTGATGGAGCCTGTGTAAAGACATGCTTGCTCATAGTCTTC
	Reverse	GAAGACTATGAGCAAGCATGTCTTTACACAGGCTCCATCACCAACAATCAC
K18N	Forward	GGTGATGGAGCCTGTGGAAACACATGCTTGCTCATAGTC
	Reverse	GACTATGAGCAAGCATGTGTTTCCACAGGCTCCATCACC
T19N	Forward	GGTGATGGAGCCTGTGGAAAGAACTGCTTGCTCATAGTCTTCAGC
	Reverse	GCTGAAGACTATGAGCAAGCAGTTCTTTCCACAGGCTCCATCACC
L22P	Forward	CTGGTCCTTGCTGAAGACTATGGGCAAGCATGTCTTTCCACAGGC
	Reverse	GCCTGTGGAAAGACATGCTTGCCCATAGTCTTCAGCAAGGACCAG
L22R	Forward	CTGGTCCTTGCTGAAGACTATGCGCAAGCATGTCTTTCCACAGGC
	Reverse	GCCTGTGGAAAGACATGCTTGCGCATAGTCTTCAGCAAGGACCAG
I23R	Forward	GGAAAGACATGCTTGCTCAGAGTCTTCAGCAAGGACCAG
	Reverse	CTGGTCCTTGCTGAAGACTCTGAGCAAGCATGTCTTTCC
Y34C	Forward	GACCAGTTCCCAGAGGTGTGTGTGCCCACAGTGTTTGAG
	Reverse	CTCAAACACTGTGGGCACACACACCTCTGGGAACTGGTC
Y34F	Forward	GACCAGTTCCCAGAGGTGTTTGTGCCCACAGTGTTTGAG
	Reverse	CTCAAACACTGTGGGCACAAACACCTCTGGGAACTGGTC

Table 2. Primers used for the generation of *RHOA* mutations by site-directed mutagenesis (continuation from page).

RHOA mutation	Primer sequence (5'►3')	
E40Q	Forward	GTGCCCACAGTGTTTCAGAACTATGTGGCAG
	Reverse	CTGCCACATAGTTCTGAAACACTGTGGGCAC
Y42C	Forward	CCCACAGTGTTTGAGAACTGTGTGGCAGATATCGAGGTG
	Reverse	CACCTCGATATCTGCCACACAGTTCTCAAACACTGTGGG
Y42F	Forward	CCCACAGTGTTTGAGAACTTTGTGGCAGATATCGAGGTG
	Reverse	CACCTCGATATCTGCCACAAAGTTCTCAAACACTGTGGG
Y42S	Forward	CCCACAGTGTTTGAGAACTCTGTGGCAGATATCGAGGTG
	Reverse	CACCTCGATATCTGCCACAGAGTTCTCAAACACTGTGGG
E47K	Forward	CTATGTGGCAGATATCAAGGTGGATGGAAAGCAG
	Reverse	CTGCTTTCCATCCACCTTGATATCTGCCACATAG
L57V	Forward	AAGCAGGTAGAGTTGGCTGTGTGGGACACAGCTGGGCAG
	Reverse	CTGCCCAGCTGTGTCCCACACAGCCAACTCTACCTGCTT
D59G	Forward	GCAGGTAGAGTTGGCTTTGTGGGGCACAGCTGGGCAGGAAGATTATG
	Reverse	CATAATCTTCCTGCCCAGCTGTGCCCCACAAAGCCAACTCTACCTGC
D59N	Forward	GCAGGTAGAGTTGGCTTTGTGGAACACAGCTGGGCAGGAAGATTATG
	Reverse	CATAATCTTCCTGCCCAGCTGTGTTCCACAAAGCCAACTCTACCTGC
T60K	Forward	GATCATAATCTTCCTGCCCAGCTTTGTCCCACAAAGCCAACTCTACC
	Reverse	GGTAGAGTTGGCTTTGTGGGACAAAGCTGGGCAGGAAGATTATGATC
A61D	Forward	GTTGGCTTTGTGGGACACAGATGGGCAGGAAGATTATGATC
	Reverse	GATCATAATCTTCCTGCCCATCTGTGTCCCACAAAGCCAAC
A61V	Forward	GTTGGCTTTGTGGGACACAGTTGGGCAGGAAGATTATGATC
	Reverse	GATCATAATCTTCCTGCCCAACTGTGTCCCACAAAGCCAAC
G62E	Forward	GGCTTTGTGGGACACAGCTGAGCAGGAAGATTATGATCGCC
	Reverse	GGCGATCATAATCTTCCTGCTCAGCTGTGTCCCACAAAGCC
G62R	Forward	GGCTTTGTGGGACACAGCTAGGCAGGAAGATTATGATCGCC
	Reverse	GGCGATCATAATCTTCCTGCCTAGCTGTGTCCCACAAAGCC
Q63K	Forward	TTGTGGGACACAGCTGGGAAGGAAGATTATGATCGCCTG
	Reverse	CAGGCGATCATAATCTTCCTTCCCAGCTGTGTCCCACAA
Q63L	Forward	TTGTGGGACACAGCTGGGCTGGAAGATTATGATCGCCTG
	Reverse	CAGGCGATCATAATCTTCCAGCCCAGCTGTGTCCCACAA
Y66D	Forward	GGAGAGGGGCCTCAGGCGATCATCATCTTCCTGCCCAGCTGTGTC
	Reverse	GACACAGCTGGGCAGGAAGATGATGATCGCCTGAGGCCCCTCTCC
Y66N	Forward	GACACAGCTGGGCAGGAAGATGATGATCGCCTGAGGCCCCTCTCC
	Reverse	GACACAGCTGGGCAGGAAGATAATGATCGCCTGAGGCCCCTCTCC
L69P	Forward	GCAGGAAGATTATGATCGCCCGAGGCCCCTCTCCTACCCAG
	Reverse	CTGGGTAGGAGAGGGGCCTCGGGCGATCATAATCTTCCTGC
L69R	Forward	GCAGGAAGATTATGATCGCCGGAGGCCCCTCTCCTACCCAG
	Reverse	CTGGGTAGGAGAGGGGCCTCCGGCGATCATAATCTTCCTGC

Table 2. Primers used for the generation of *RHOA* mutations by site-directed mutagenesis (continuation from page).

RHOA mutation	Primer sequence (5'►3')	
R70K	Forward	CGGTATCTGGGTAGGAGAGGGGCTTCAGGCGATCATAATCTTCCTGCC
	Reverse	GGCAGGAAGATTATGATCGCCTGAAGCCCCTCTCCTACCCAGATACCG
R70S	Forward	CGGTATCTGGGTAGGAGAGGGGGCTCAGGCGATCATAATCTTCCTGCC
	Reverse	GGCAGGAAGATTATGATCGCCTGAGCCCCCTCTCCTACCCAGATACCG
P75L	Forward	CATCAGTATAACATCGGTATCTAGGTAGGAGAGGGGCCTCAGGCG
	Reverse	CGCCTGAGGCCCCTCTCCTACCTAGATACCGATGTTATACTGATG
P75R	Forward	CATCAGTATAACATCGGTATCTCGGTAGGAGAGGGGCCTCAGGCG
	Reverse	CGCCTGAGGCCCCTCTCCTACCGAGATACCGATGTTATACTGATG
N117I	Forward	CCCATCATCCTGGTTGGGATTAAGAAGGATCTTCGG
	Reverse	CCGAAGATCCTTCTTAATCCCAACCAGGATGATGGG
N117K	Forward	CCCATCATCCTGGTTGGGAAAAAGAAGGATCTTCGG
	Reverse	CCGAAGATCCTTCTTTTTCCCAACCAGGATGATGGG
K118E	Forward	CCCATCATCCTGGTTGGGAATGAGAAGGATCTTCGGAATGATG
	Reverse	CATCATTCCGAAGATCCTTCTCATTCCCAACCAGGATGATGGG
A161E	Forward	GCTTTTGGGTACATGGAGTGTTCAGAAAAGACCAAAGATGGAGTGAGAGAG
	Reverse	CTCTCTCACTCCATCTTTGGTCTTTTCTGAACACTCCATGTACCCAAAAGC
A161P	Forward	GCTTTTGGGTACATGGAGTGTTCACCAAAGACCAAAGATGGAGTGAGAGAG
	Reverse	CTCTCTCACTCCATCTTTGGTCTTTGGTGAACACTCCATGTACCCAAAAGC
ΔCAAL	Forward	GGAAGAAAAAATCTGGTTGACTTGTCTTGTGAGAATTCG
	Reverse	CGAATTCTCACAAGACAAGTCAACCAGATTTTTTCTTCC
-SAAL	Forward	GGAAGAAAAAATCTGGGTCCCTTGTCTTGTGA
	Reverse	TCACAAGACAAGGGACCCAGATTTTTTCTTCC

CELL LINES

Jurkat cells were purchased from ATCC and grown in RPMI-1640 medium supplemented with 10% Fetal Bovine Serum (FBS), 1% L-glutamine, penicillin (10 µg/ml) and streptomycin (100 µg/ml). COS1, HEK293 and NIH-3T3 cells were grown in DMEM medium supplemented with 10% FBS, 1% L-glutamine, penicillin (10 µg/ml) and streptomycin (100 µg/ml). All tissue culture reagents were obtained from Gibco-Thermo Fisher Scientific. All cell lines were maintained at 37ºC in a humidified, 5% CO_2 atmosphere.

LUCIFERASE REPORTER ASSAYS

For SRF and STAT3 experiments, exponentially growing COS1 cells in 6-wells plates were transfected with 1 µg of the pSRE-Luc or pSTAT3-luc plasmids, 1 ng of pRL-SV40

plasmid encoding the *Renilla* luciferase, and 1 μg of the appropriate experimental vectors using the jetPEI reagent (Cat. No. 101000020, Polyplus). After 36 hours, cells were lysed with Passive Lysis Buffer (Cat No. E1960, Promega) and luciferase activities determined using the Dual Luciferase Assay System (Cat No. E1960, Promega) in a GloMax Navigator System (Promega). For NFAT, AP-1, HES1, and NF-kB assays, $2x10^7$ of exponentially growing Jurkat cells were co-electroporated (250V, 950 μF pulses) with the pNFAT-luc, pHes1-luc, pAP1-luc, or pNF-κB-luc reporter vector (10 μg), the pRL-SV40 Renilla vector (5 ng), and 20 μg of the appropriate *RHOA*-encoding experimental vectors using a Gene Pulser II apparatus (Cat. #165–2106; BioRad). For NFAT and NF-κB, 48 hours post-transfection cells were either non-stimulated or stimulated for 8 hours with antibodies against human CD3 (UCHT1 clone, Cat. No. 217570, Calbiochem, 5 μg/ml) in the case of NFAT, or with antibodies against human CD3 and mouse CD28 (Cat. No. 102102, BioLegend; 1 mg/ml) in the case of NF-κB. For AP-1, 24 hours upon transfection the cells were stimulated or non-stimulated with PMA (Cat. number P1585, Sigma; 20 ng/ml) for 24 hours. In all the assays cells were then lysed with Passive Lysis Buffer and luciferase activities were determined using the Dual Luciferase Assay System as above. In all cases, we normalized the firefly luciferase activity obtained in each experimental point to the activity of the *Renilla* luciferase obtained in each sample. Moreover, we checked the correct expression of the ectopically expressed proteins interrogated in the experiments in aliquots of the lysates by Western blot. Values are represented in graphs as the *n*-fold change in the experimental sample relative to the activity shown by mock-transfected cells (which was given an arbitrary value of 1 in each case).

WESTERN BLOT ANALYSES

To determine the abundance of proteins, cells were washed with phosphate-buffered saline (PBS) solution and lysed in lysis buffer (10 mM Tris–HCl [pH 7.5], 150 mM NaCl, 1% Triton X-100 (Cat. number X100, Sigma), 1 mM Na_3VO_4 (Cat. number S6508, Sigma), 10 mM β-glycerophosphate (Cat. number 50020, Sigma-Aldrich), and a cocktail of protease inhibitors [Cømplete, Cat. No. 05056489001, Roche]). Cellular extracts were precleared by centrifugation at 14000 rpm for 10 min at 4ºC, denaturalized by boiling in SDS-PAGE buffer, separated electrophoretically, and transferred into nitrocellulose filters ((Cat. No. 2022-04-26, Thermo Fisher) using the iBlot Dry Blotting System

(Thermo Fisher). Membranes were blocked in 5% bovine serum albumin (Cat. No. A4503, Sigma-Aldrich) in TBS-T (25 mM Tris–HCl [pH 8.0], 150 mM NaCl, 0.1% Tween-20 (Cat. number P7949, Sigma)) for at least 1 h and then incubated 2 hours at room temperature or overnight at 4ºC with the proper primary antibodies (**Table 3**). Then, membranes were washed three times with TBS-T, incubated with the appropriate secondary antibody (1:5000 dilution, GE Healthcare) for 45 min at room temperature, and washed twice as above. Immunoreacting bands were developed using a conventional chemiluminescent method (ECL, Cat. No. RPN2209, Amersham).

Table 3. Primary antibodies used for expression analyses

Antibody	Description	Dilution	Reference
RHOA	RhoA (67B9) Rabbit mAb	1:1000	CST, Cat. #2117
GFP	Purified anti-GFP Epitope Tag Antibody	1:2000	Biolegend, Cat. #902601
AU5	AU5 Monoclonal Antibody	1:1000	Covance, Cat. MMS-135R
Tubulin α	Anti-α-Tubulin Mouse mAb (DM1A)	1:2000	Calbiochem, Cat. #CP06
RAP1GDS1	RAP1GDS1 (F-1) Mouse mAb	1:1000	SCBT, Cat. #sc-390003
VAV1 DH	Homemade Polyclonal antibody	1:10,000	Ref. 302-5
PLCγ1	Anti-PLCγ1 Rabbit Polyclonal Antibody	1:1000	CST, Cat. #2822
SLP76	Anti-SLP-76 Rabbit Polyclonal Antibody	1:1000	CST, Cat. #4958
GAPDH	Anti-GAPDH (FL-335) Mouse mAb	1:2000	SCBT, Cat. #sc-25778
RHOGDIα	Anti-RhoGDIα (A-20) Rabbit Polyclonal	1:1000	SCBT, Cat. #sc-360
HA	HA-Tag (C29F4) Rabbit mAb	1:1000	CST, Cat. #3724
LAT	LAT (E3U6J) XP® Rabbit mAb	1:1000	CST, Cat. #45533
RAC1	Purified mouse anti-Rac1	1:1000	BD Biosciences, Cat. #610651
CDC42	CDC42 (P1) Rabbit Polyclonal	1:1000	SCBT, Cat. #sc-87

GENERATION OF HEATMAP REPRESENTATIONS

For heatmap representations, we used the heatmap3 R package including the activities SRF and NFAT, as well as the interaction with the proteins RHOGDIα and RAP1GDS1 analyzed in this study for all the *RHOA* mutations tested, assigning to the values obtained with $RHOA^{WT}$ an arbitrary number of 1.

GENERATION OF STABLE CELL LINES

Pulls ectopically expressing the indicated RHOA mutants were generated using a retroviral delivery method. To generate the retroviral particles, 5 μg of pMD-G, 7.5 μg of pNGVL-MLV-gag-pol, and 10 μg of the appropriate retroviral plasmid (pMIEG3) were transfected into HEK293T cells using jetPEI reagent according to the manufacturer's instructions. Cell culture supernatants were collected 24, 48 and 72 hours later, and passed through 0.45 μm filters (Cat. #10462100, GE Healthcare). Jurkat cells were infected with the retroviral particles generated supplemented with polybrene (8 μg/ml, Cat. #H9268, Sigma) by spinoculation at 1,800 rpm for 90 min at room temperature. The GFP^+ population was selected by flow cytometry in a FACS Aria III flow cytometer (BD Biosciences). Proper protein expression was assessed by Western blot.

IMMUNOPRECIPITATION

Exponentially growing COS1 cells plated in 10-cm plates were transfected with 10 μg of plasmid containing the different GTP-bound RHOA mutations by using the diethylaminoethyl-dextran (10 mg/mL, Cat. #D9885, Sigma)/chloroquine (2.5 mM, Cat. #C6628, Sigma) method [149]. 48 hours upon transfection, cells were washed in a phosphate-buffered saline solution and lysed in 1 ml of the lysis buffer indicated above with the help of a scrapper. Cell lysates were kept 10 min on ice and centrifuged at 14,000 rpm for 10 min at 4°C to eliminate cell debris. The supernatants were then incubated with 3 μl of GFP-Trap reagent (Cat. No. GTA-100, ChromoTek) for 2 hours at 4°C. Then, 20 ml of Glutathione-Sepharose beads (Cat. #17-0756-01, GE Healthcare) were added to each sample and washed three times with a lysis buffer. The immunocomplexes were collected by centrifugation and subjected to immunoblot analyses as above.

In the case of Jurkat cells, 2 x 10^7 cells were transfected (250V, 950 μF pulses) with 20 μg of plasmid of interest per sample. 48 hours post-transfection, cells were washed and transferred to a 1.5 mL Eppendorf tube, where they were resuspended in 1 ml of lysis buffer and incubated on ice for 10 min. The supernatants were then incubated with 3 μl of GFP-Trap reagent. The cell extracts obtained were processed as above. In all cases, total cellular lysates were analyzed in parallel to monitor the expression of the ectopically expressed proteins used in each experiment and the analyses of total cellular lysates were performed in parallel to detect the expression of the indicated proteins.

PROTEOMIC ANALYSIS

Jurkat stable cell lines expressing HA-tagged $RHOA^{WT}$, $RHOA^{C16R}$ and $RHOA^{G17V}$ were either non-stimulated or stimulated with antibodies against human CD3 for 10 min at 37ºC. Cells were then washed with phosphate-buffered saline solution and lysed with lysis buffer (10 mM Tris-HCl (pH 7.5), 150 mM NaCl, 1% Triton X-100, 1 mM Na_3VO_4, 10 mM EDTA, 10 mM EGTA, 10 mM DTT, 1 mM PMSF, 10 mM β-glycerophosphate and Cømplete). Cell lysates were incubated on ice for at least 10 min, clarified by centrifuge at 14,000 rpm for 10 min at 4ºC and incubated with anti-HA magnetic beads (Cat. #88836, Thermo Fisher Scientific) for 2 hours at 4ºC. Immunocomplexes were collected with Gammabind GSepharose beads (Cat. # GE17-0885-01; GE Healthcare), washed three times in lysis buffer, resuspended in SDS-PAGE buffer, boiled for 5 min, and subjected to one-dimensional SDS-PAGE electrophoresis. Then, the protein bands in the polyacrylamide gel were visualized by silver staining [150], manually excised, and subjected to in-gel trypsin digestion [151]. The resulting peptides from trypsin digestion were acidified with TFA to a final concentration of 0.2% and concentrated and desalted using reverse-phase chromatography on Empore SDB-XC microcolumns [152]. The eluted peptides were dried in a SpeedVac (Eppendorf) and resuspended for mass spectrometry analysis in 0.1% formic acid (FA), 2% acetonitrile (ACN). The samples were analyzed using LC-MS/MS (Liquid Chromatography-Mass Spectrometry) with a nanoUPLC system (NanoElute, Bruker). A precolumn Trap AcclaimPepMap 100 C18 (Thermo) and a C18 1.9 μm 75 ID 15 cm column (BRUKER FIFTEEN, Bruker) were employed. The LC system was connected to a TIMSTOF Pro mass spectrometer (Bruker). The analysis was carried out using a gradient of 2% to 35% ACN with 0.1% FA over a period of 15 minutes. The analysis of the obtained data was carried out using the MaxQuant software with the Andrómeda search engine against the complete proteome database of Homo sapiens (Organism ID 0906) and common contaminant sequences included in the MaxQuant program [153]. For peptide and protein identification, peptides with a minimum length of six amino acids were considered, and a 1% false discovery rate (FDR) at both the peptide and protein levels was applied using a search strategy against a reversed sequence library. To calculate the relative abundance of each protein, the iBAQ algorithm was employed [154].

shRNA-MEDIATED TRANSCRIPT KNOCKDOWNS

Jurkat cells were infected with lentiviruses encoding either scrambled (TR1.5-pLKO-1-puro, Sigma) or *RAP1GDS1*-directed shRNAs (TRCN0000029790 [referred to in the figure as sh1], TRCN0000029792 [referred to in the figure as sh2]). To generate the lentiviral particles, 5 µg of pMD-G, 7.5 µg of pPAX2, and 10 µg of the appropriate lentiviral plasmid were transfected into HEK293T cells using jetPEI reagent according to the manufacturer's instructions. Cell culture supernatants were collected 24, 48 and 72 hours later, and passed through 0.45 µm filters. Jurkat cells were infected with the lentiviral particles generated supplemented with Polybrene (8 µg/ml) by spinoculation at 1,800 rpm for 90 min at room temperature and subjected to puromycin selection for 15 days. Then, following the identification of pools exhibiting lower *RAP1GDS1* expression, single-cell isolation was conducted to obtain individual clones. The proper transcription knockdown was assessed using immunoblotting and qRT-PCR.

DETERMINATION OF mRNA ABUNDANCE

Total RNA was extracted from cells using NZYol (Cat. No. MB18501, NZYtech) and mRNAs purified using RNeasy Mini Kit (Cat. No. 74106, QIAGEN) following the manufacturer's instructions. mRNAs were analyzed by qRT–PCR using the iScript One-Step RT–PCR kit with SYBR green (Cat. No. 1708892, Bio-Rad) and the StepOnePlus Real-Time PCR System (Applied BioSystems) using the primers in **Table 4**. Raw qRT-PCR data were analyzed using the StepOne software v2.1 (Applied Biosystems). The abundance of the endogenous *GAPDH* was used as internal normalization control.

Table 4.Primers used for gene expression analyses

Gene	Primer sequence (5'►3')	
VAV1	Forward	TGGTGTCCTTCTGTGTCAGC
	Reverse	CTTGAGGCCGAACTTCTCAC
RAP1GDS1	Forward	TCCATGTGTGGATGCTGGATTGA
	Reverse	TGCATTTTGGCAGTGGATGC
GAPDH	Forward	ATGGCCTTCCGTGTCCCCACTG
	Reverse	TGAGTGTGGCAGGGACTCCCCA

PRODUCTION OF RETROVIRAL PARTICLES

To generate the retroviral particles needed to the viral transduction of primary mouse $CD4^+$ T cells, the retroviral plasmids together with the pCL-Eco packaging vector were transfected into HEK293T cells using the JetPEI transfection reagent (Cat. No. 101-10N, Polyplus). The medium containing the viruses were collected and concentrated using Lenti-X™ concentrator (Cat. No. 631231, Takara) by centrifuging at 2,400 rpm for 45 min at 4°C. Concentrated retroviruses were resuspended and tittered by infecting NIH3T3 cells and scoring GFP-positive cells by flow cytometry. Viruses with high titers were aliquoted and stored in -80°C for up to 3 months.

$CD4^+$ T-CELL ISOLATION AND ACTIVATION

Spleen and lymph nodes were mechanically homogenized in 5 ml of phosphate-buffered saline solution supplemented with 2% bovine serum albumin and 0.5 mM EDTA (referred from now on as cell extraction buffer) to obtain single-cell resuspensions. These cells were washed once by low-speed centrifugation, subjected to a 0.17 M NH_4Cl lysis step to remove erythrocytes, and filtered with a cell sieve (nylon mesh with 40-µm pores, Cat. No. 352340, Falcon) to eliminate debris. Naïve $CD4^+$ T cells were purified by negative selection using the EasySep™ Mouse $CD4^+$ T Cell Isolation Kit (Cat. No. 19852, StemCell Technologies) following the manufacturer's instructions. Then, 1×10^6 of purified $CD4^+$ T cells were cultured on goat-anti-hamster IgG (Cat. No. 31115, Invitrogen)-coated plates for 16–24 h in RPMI-1640 media containing 10% fetal bovine serum, L-glutamine, 50 µM 2-mercaptoethanol, antibodies to CD3 (Cat. No. 100202, BioLegend; 1 µg/ml), and antibodies to CD28 (Cat. No. 102102, BioLegend; 0.5 µg/ml). The quality of the purification step was confirmed by flow cytometry.

ECTOPIC EXPRESSION OF RHOA MUTANTS IN $CD4^+$ T CELLS

As indicated above, $CD4^+$ T cells were stimulated with antibodies to CD3 and CD28 for 16 h. Then, they were infected with retroviruses encoding the indicated proteins in presence of polybrene (6 µg/ml; Cat. No. H9268-5G, Sigma-Aldrich), pelleted by centrifugation (2400 rpm at 32°C for 90 min), and treated with interleukin 2 (Cat. No. 200-02, PeproTech; 50 U/ml). The transduction efficiency was observed 48 h after transduction by flow cytometry. Transduced cells were used either for short-term cell cultures or for adoptive T-cell transfer experiments as indicated below.

EVALUATION OF SHORT-TERM EFFECTS OF RHOA MUTATIONS IN CD4$^+$ T CELLS

CD4$^+$ T cells purified from spleen and lymph nodes as above were stained with Cell Trace Violet (Cat. number C34557, Life Technologies) following the instructions provided by the manufacturer. Then, cells were cultured on goat anti-hamster IgG-coated plates for 16-14 h in RPMI media and stimulated as above. Upon activation, cells were infected with the indicated retroviral particles in the presence of IL-2 (50 U/ml) as above and, three days later, were processed to measure the indicated biological and signaling parameters by flow cytometry.

FLOW CYTOMETRY DETERMINATION OF SURFACE AND INTRACELLULAR PROTEINS

For surface proteins, isolated cells were washed with cell extraction buffer, resuspended in standard phosphate-buffered saline solution, and stained following standard procedures with combinations of the antibodies enlisted in **Table 5**.

For intracellular BCL6, T-BET, and GATA3 staining, cells were fixed with Fixation/Permeabilization working solution (Cat. number 00-5123-43, Invitrogen), permeabilized with Permeabilization Buffer (Cat. number 00-8333-56, Invitrogen), and stained with the correspondent antibodies in **Table 5** For flow cytometry detection of phosphorylated intracellular proteins, cells were stimulated with antibodies against CD3 (2 μg/ml) and CD28 (2 μg/ml) and IgG (20 μg/ml) for 20 minutes at 37°C. Then, cells were fixed with 2% formaldehyde (Cat. #F8775, Sigma), permeabilized with 90% ice-cold methanol, and incubated with a combination of the antibodies in **Table 5**. In all cases, antibody-stained cells were run in a FACSAria III flow cytometer (BD Biosciences) and data analyzed using the FlowJo software.

Table 5. Antibodies used for flow cytometry determination

Antibody	Description	Dilution	Reference
CD4	FITC Rat Anti-Mouse CD4	1:200	BD Pharmingen, Cat. # 553729
CD4	PerCP-Cyanine5.5 Anti-Mouse CD4	1:200	Invitrogen, Cat. # 45-0042-82
CD4	APC Anti-Mouse CD4	1:200	Invitrogen, Cat. # 17-0042-83
CD8	Pacific Blue Rat Anti-Mouse CD8a	1:200	BD Pharmingen, Cat. # 558106
CD8	FITC Anti-Mouse CD8a	1:200	Invitrogen, Cat. # 11-0081-82
PD-1	PE Anti-Mouse CD279 (PD-1)	1:200	Invitrogen, Cat. # 12-9985-82
CXCR5	PE-Cyanine7 Anti-Mouse CD185 (CXCR5)	1:200	Invitrogen, Cat. # 25-7185-82
ICOS	APC Anti-Mouse/Rat CD278 (ICOS)	1:200	Invitrogen, Cat. # 17-9949-82
B220	PerCP-Cyanine5.5 Anti-Hu/Mo CD45R (B220)	1:200	Invitrogen, Cat. # 45-0452-82
CD69	PerCP-Cyanine5.5 Anti-Mouse CD69	1:200	Invitrogen, Cat. # 45-0691-82
CD25	PE-Cyanine7 Anti-Mouse CD25	1:200	BD Pharmingen, Cat. # 552880
BCL6	APC Anti-Mouse BCL6	1:50	Invitrogen, Cat. # 17-5453-82
T-BET	PerCP-Cyanine5.5 Anti-Human/Mouse T-bet	1:50	Invitrogen, Cat. # 45-5825-82
GATA3	PE Anti-Human/Mouse Gata-3	1:50	Invitrogen, Cat. # 12-9966-42
pErk1/2$^{Thr202/Tyr204}$	PerCP Monoclonal Phospho-ERK1/2 (T202, Y204)	1:50	Invitrogen, Cat. # 46-9109-42
pS6$^{Ser235/Ser236}$	PE Monoclonal Phospho-S6 (S235, S236)	1:50	Invitrogen, Cat. # 12-9007-42

ADOPTIVE T-CELL TRANSFER EXPERIMENTS

24 h after the retroviral transduction step, the EGFP^{+} CD4^{+} T cells were collected by centrifugation (1200 rpm for 5 min) and resuspended in phosphate-buffered saline solution at a concentration of 1 x 10^{4} cells/µl. Then, 100 µl of the cell resuspension was introduced by retro-orbital injection into 6- to 8-week-old *Tet*$^{-/-}$ recipient mice. Mice were then examined weekly until showing noticeable physical signs of sickness. Aliquots of peripheral blood (100 µl) were analyzed by flow cytometry to detect changes in immune populations. Upon euthanasia, the indicated tissues and peripheral blood were collected for histological processing, flow cytometry analyses, and extraction of either total cellular proteins or RNAs.

IN VIVO PHARMACOLOGICAL TREATMENTS

To test the effect of Calcineurin inhibition in tumor cell development we used the compound FK506 (Cat. number tlrl-fk5, Invitrogen) into recipient mice transplanted with GFP- or $RHOA^{G17V}$-expressing *Tet2*$^{-/-}$ $CD4^+$ T cells. FK506 was dissolved in DMSO and diluted 1:10 in phosphate buffered saline solution and administered subcutaneously at a dose of 2.5 mg/kg every day for two weeks, doing a total of two rounds of 14 days with a break during one week between the two rounds. Animals were randomly assigned to two treatment cohorts, vehicle only (n = 5) or FK506 (n = 7). The effect of the treatment was assessed by checking the levels of GFP^+ T cells in peripheral blood by FACs and the quantification of spleen weight after euthanasia.

HISTOLOGICAL ANALYSIS AND IMMUNOHISTOCHEMISTRY

Mouse tissues were dissected and fixed in 4% paraformaldehyde in phosphate-buffered saline solution, paraffin-embedded, cut in 2-3 mm sections and subjected to hematoxylin-eosin staining using the standard procedures.

Immunohistochemical staining was performed using a Ventana Discovery Ultra instrument (Roche, Cat. # 05987750001). Paraffin–embedded sections were dewaxed, subjected to either citrate buffer [pH 6.0] for heat–induced antigen retrieval, and incubated overnight with primary antibodies to Ki67 (Cat. number MAD-000310QD, Master Diagnostica), CD4 (clone EPR19514; Cat. number AB183685, Abcam), CD31 (Cat. number AB28364, Abcam), and Caspase-3 (E-AB-13815, Elabscience) at 4°C. Sections were then incubated with biotin-conjugated secondary antibodies followed by the addition of the Vectastain Elite ABC reagent (Cat.No. PK-6100; Vector Laboratories, Burlingame, CA,USA). The reaction product was visualized by incubating the sections in 0.025% 3.30-diaminobenzidine and 0.003% H_2O_2 in phosphate-buffered saline solution.

APOPTOSIS ANALYSIS

Aliquots of peripheral blood from recipient mice transplanted with GFP- or $RHOA^{G17V}$-expressing $CD4^+$ T cells and treated with the inhibitor FK506 were collected and washed with ACK buffer to remove the erythrocytes. Cells were stained using the CFBlue Annexin V Apoptosis Detection Kit (Cat. number ANXVKCFB7-110T, Immunostep,

Salamanca, Spain) following the manufacturer's instructions, and the number of GFP^+ apoptotic cells was measured by flow cytometry using a FACSAria III flow cytometer (BD Biosciences) and data analyzed using the FlowJo software.

AMPLIFICATION OF MOUSE PRIMARY CELL LINES

Leukemic cells from *Tet2*$^{-/-}$;*RHOA*^{G17V} mice were processed for flow cytometry characterization and rapidly stored in liquid nitrogen resuspended in FBS containing 10% of dimethyl sulfoxide (DMSO). For expansion, cells were thawed and injected into sublethally-irradiated 6- to 8- week-old NSG mice. Peripheral blood was checked every week to detect the presence of GFP^+ cells and, when they reached 90% of the blood population, mice were euthanized. GFP^+ T cells were collected from spleen and lymph nodes and frozen in liquid nitrogen until needed.

IN VITRO PHARMACOLOGICAL TREATMENTS

Leukemic cells were cultured for 3 days in RPMI medium and were randomly assigned to five treatment cohorts: PBS solution, 10 μM FK506, 1 μg/ml α-ICOSL (Cat. number BE0028, InVivoMAb), 200 nM Wortmannin (Cat. number S2758, Selleckchem) and 200 nM Compound E (Cat. number ALX-270-415-C250, Enzo Life Sciences). The relative number of cells was measured every day by flow cytometry. On the third day the percentage of apoptotic cells was measured.

ETHICS STATEMENT

All mouse experiments were performed according to protocols approved by the Bioethics Committee of the university of Salamanca and the animal experimental authorities of the autonomous Government of Castilla y León (Spain). No statistical methods were used to determine sample size. In all cases, we have used at least five mice per experiment. The exact sample size used in each experiment is indicated in the appropriate figure legend of the manuscript.

STATISTICAL ANALYSES

Microsoft Excel 2020 (Microsoft, Redmond, WA, USA) and GraphPad Prism software (version 6.0; Dotmatics, Boston, MA, USA) were used to perform calculations. The number of biological replicates (n), the type of statistical tests performed, and the

statistical significance for each experiment are indicated in the figure legends. Parametric and nonparametric distributions were analyzed using Student's t-test and Mann–Whitney test, respectively. Chi-squared tests were used to determine the significance of the differences between expected and observed frequencies. Statistical analyses of the immunoblot-generated data were carried out using the GraphPad Prism software (version 6.0). In all cases, values were considered significant when $P \leq 0.05$. Data obtained are given as the mean ± SEM.

CONCLUSIONS

The research provided in this Ph.D. thesis suggests that based on the preceding findings:

1. *RHOA* mutations in peripheral T-cell lymphomas show a neomorphic effect, which is mediated by:
    a) Defective prenylation
    b) Increased RAP1GDS1 binding
    c) RAP1GDS1-dependent interactions with the PLCγ1 signalosome

2. RHOA neomorphic mutants promote proliferation in primary cells in a RAP1GDS1-dependent manner

3. $RHOA^{G17V}$- lymphomagenesis is NFAT-dependent.

BIBLIOGRAPHY

1. Jaffe, A.B. and A. Hall, *Rho GTPases: biochemistry and biology.* Annu Rev Cell Dev Biol, 2005. **21**: p. 247-69.

2. Haga, R.B. and A.J. Ridley, *Rho GTPases: Regulation and roles in cancer cell biology.* Small GTPases, 2016. **7**(4): p. 207-221.

3. Heasman, S.J. and A.J. Ridley, *Mammalian Rho GTPases: new insights into their functions from in vivo studies.* Nat Rev Mol Cell Biol, 2008. **9**(9): p. 690-701.

4. Colicelli, J., *Human RAS superfamily proteins and related GTPases.* Sci STKE, 2004. **2004**(250): p. RE13.

5. Schaefer, A., N.R. Reinhard, and P.L. Hordijk, *Toward understanding RhoGTPase specificity: structure, function and local activation.* Small GTPases, 2014. **5**(2): p. 6.

6. Orgaz, J.L. and V. Sanz-Moreno, *RhoA*, in *Encyclopedia of Signaling Molecules*. 2016, Springer New York. p. 1-11.

7. Wheeler, A.P. and A.J. Ridley, *Why three Rho proteins? RhoA, RhoB, RhoC, and cell motility.* Exp Cell Res, 2004. **301**(1): p. 43-9.

8. Hodge, R.G. and A.J. Ridley, *Regulating Rho GTPases and their regulators.* Nat Rev Mol Cell Biol, 2016. **17**(8): p. 496-510.

9. Bustelo, X.R., V. Sauzeau, and I.M. Berenjeno, *GTP-binding proteins of the Rho/Rac family: regulation, effectors and functions in vivo.* Bioessays, 2007. **29**(4): p. 356-70.

10. Bourne, H.R., D.A. Sanders, and F. McCormick, *The GTPase superfamily: conserved structure and molecular mechanism.* Nature, 1991. **349**(6305): p. 117-27.

11. Ueyama, T., *Rho-Family Small GTPases: From Highly Polarized Sensory Neurons to Cancer Cells.* Cells, 2019. **8**(2).

12. Møller, L.L.V., A. Klip, and L. Sylow, *Rho GTPases-Emerging Regulators of Glucose Homeostasis and Metabolic Health.* Cells, 2019. **8**(5).

13. Olson, M.F., *Rho GTPases, their post-translational modifications, disease-associated mutations and pharmacological inhibitors.* Small GTPases, 2018. **9**(3): p. 203-215.

14. Tang, J., et al., *Cdk5-dependent Mst3 phosphorylation and activity regulate neuronal migration through RhoA inhibition.* J Neurosci, 2014. **34**(22): p. 7425-36.

15. Uezu, A., et al., *Modified SH2 domain to phototrap and identify phosphotyrosine proteins from subcellular sites within cells.* Proc Natl Acad Sci U S A, 2012. **109**(43): p. E2929-38.

16. Tong, J., et al., *Phosphorylation and Activation of RhoA by ERK in Response to Epidermal Growth Factor Stimulation.* PLoS One, 2016. **11**(1): p. e0147103.

17. Kim, J.G., et al., *Tyr42 phosphorylation of RhoA GTPase promotes tumorigenesis through nuclear factor (NF)-κB.* Free Radic Biol Med, 2017. **112**: p. 69-83.

18. Liu, J., et al., *c-Met-dependent phosphorylation of RhoA plays a key role in gastric cancer tumorigenesis.* J Pathol, 2019. **249**(1): p. 126-136.

19. Rafikov, R., et al., *Lipopolysaccharide-induced lung injury involves the nitration-mediated activation of RhoA.* J Biol Chem, 2014. **289**(8): p. 4710-22.

20. Worby, C.A., et al., *The fic domain: regulation of cell signaling by adenylylation.* Mol Cell, 2009. **34**(1): p. 93-103.

21. Heo, J., et al., *Redox regulation of RhoA.* Biochemistry, 2006. **45**(48): p. 14481-9.

22. Schmidt, G., et al., *Lysine and polyamines are substrates for transglutamination of Rho by the Bordetella dermonecrotic toxin.* Infect Immun, 2001. **69**(12): p. 7663-70.

23. Singh, U.S., *Role of transglutaminase II in retinoic acid-induced activation of RhoA-associated kinase-2.* The EMBO Journal, 2001. **20**(10): p. 2413-2423.

24. Kim, J.G., et al., *Regulation of RhoA GTPase and various transcription factors in the RhoA pathway.* J Cell Physiol, 2018. **233**(9): p. 6381-6392.

25. Nomikou, E., et al., *Transcriptional and post-transcriptional regulation of the genes encoding the small GTPases RhoA, RhoB, and RhoC: implications for the pathogenesis of human diseases.* Cellular and Molecular Life Sciences, 2018. **75**(12): p. 2111-2124.

26. Schmidt, S.I., et al., *RhoA Signaling in Neurodegenerative Diseases.* Cells, 2022. **11**(9): p. 1520.

27. Cherfils, J. and M. Zeghouf, *Regulation of small GTPases by GEFs, GAPs, and GDIs.* Physiol Rev, 2013. **93**(1): p. 269-309.

28. Aspenström, P., *Activated Rho GTPases in Cancer-The Beginning of a New Paradigm.* Int J Mol Sci, 2018. **19**(12).

29. Patel, M. and A.V. Karginov, *Phosphorylation-mediated regulation of GEFs for RhoA.* Cell Adhesion & Migration, 2014. **8**(1): p. 11-18.

30. Bagci, H., et al., *Mapping the proximity interaction network of the Rho-family GTPases reveals signalling pathways and regulatory mechanisms.* Nat Cell Biol, 2020. **22**(1): p. 120-134.

31. Peifer, M., S. Berg, and A.B. Reynolds, *A repeating amino acid motif shared by proteins with diverse cellular roles.* Cell, 1994. **76**(5): p. 789-91.

32. Shimizu, H., et al., *Structure-based analysis of the guanine nucleotide exchange factor SmgGDS reveals armadillo-repeat motifs and key regions for activity and GTPase binding.* J Biol Chem, 2017. **292**(32): p. 13441-13448.

33. Vikis, H.G., S. Stewart, and K.L. Guan, *SmgGDS displays differential binding and exchange activity towards different Ras isoforms.* Oncogene, 2002. **21**(15): p. 2425-32.

34. Hamel, B., et al., *SmgGDS is a guanine nucleotide exchange factor that specifically activates RhoA and RhoC.* J Biol Chem, 2011. **286**(14): p. 12141-8.

35. Berg, T.J., et al., *Splice variants of SmgGDS control small GTPase prenylation and membrane localization.* J Biol Chem, 2010. **285**(46): p. 35255-66.

36. Brandt, A.C., O.J. Koehn, and C.L. Williams, *SmgGDS: An Emerging Master Regulator of Prenylation and Trafficking by Small GTPases in the Ras and Rho Families.* Front Mol Biosci, 2021. **8**: p. 685135.

37. Mosaddeghzadeh, N. and M.R. Ahmadian, *The RHO Family GTPases: Mechanisms of Regulation and Signaling.* Cells, 2021. **10**(7): p. 1831.

38. Garcia-Mata, R., E. Boulter, and K. Burridge, *The 'invisible hand': regulation of RHO GTPases by RHOGDIs.* Nat Rev Mol Cell Biol, 2011. **12**(8): p. 493-504.

39. Ahmad Mokhtar, A.M.B., et al., *A Complete Survey of RhoGDI Targets Reveals Novel Interactions with Atypical Small GTPases.* Biochemistry, 2021. **60**(19): p. 1533-1551.

40. Mosaddeghzadeh, N., et al., *Electrostatic Forces Mediate the Specificity of RHO GTPase-GDI Interactions.* International Journal of Molecular Sciences, 2021. **22**(22): p. 12493.

41. Liu, W., et al., *RhoGDI2 positively regulates the Rho GTPases activation in response to the β2 outside-in signaling in T cells adhesion and migration on ICAM-1*. J Leukoc Biol, 2019. **106**(2): p. 431-446.

42. Luo, J., et al., *Rho GDP-Dissociation Inhibitor 2 Inhibits C-X-C Chemokine Receptor Type 4-Mediated Acute Lymphoblastic Leukemia Cell Migration.* Front Oncol, 2020. **10**: p. 1512.

43. Lv, Z., et al., *Role of RHO family interacting cell polarization regulators (RIPORs) in health and disease: Recent advances and prospects.* International Journal of Biological Sciences, 2022. **18**(2): p. 800-808.

44. Piekny, A., M. Werner, and M. Glotzer, *Cytokinesis: welcome to the Rho zone*. Trends Cell Biol, 2005. **15**(12): p. 651-8.

45. Naydenov, N.G., J.E. Koblinski, and A.I. Ivanov, *Anillin is an emerging regulator of tumorigenesis, acting as a cortical cytoskeletal scaffold and a nuclear*

modulator of cancer cell differentiation. Cell Mol Life Sci, 2021. **78**(2): p. 621-633.

46. Long, M. and J.C. Simpson, *Rho GTPases operating at the Golgi complex: Implications for membrane traffic and cancer biology.* Tissue Cell, 2017. **49**(2 Pt A): p. 163-169.

47. Mysior, M.M. and J.C. Simpson, *Emerging roles for Rho GTPases operating at the Golgi complex.* Small GTPases, 2021. **12**(5-6): p. 311-322.

48. Croisé, P., et al., *Rho GTPases, phosphoinositides, and actin: a tripartite framework for efficient vesicular trafficking.* Small GTPases, 2014. **5**: p. e29469.

49. Villalonga, P. and A.J. Ridley, *Rho GTPases and cell cycle control.* Growth Factors, 2006. **24**(3): p. 159-64.

50. Oude Weernink, P.A., M. López De Jesús, and M. Schmidt, *Phospholipase D signaling: orchestration by PIP2 and small GTPases.* Naunyn-Schmiedeberg's Archives of Pharmacology, 2007. **374**(5-6): p. 399-411.

51. Pochynyuk, O., J.D. Stockand, and A. Staruschenko, *Ion channel regulation by Ras, Rho, and Rab small GTPases.* Exp Biol Med (Maywood), 2007. **232**(10): p. 1258-65.

52. Stankiewicz, T.R. and D.A. Linseman, *Rho family GTPases: key players in neuronal development, neuronal survival, and neurodegeneration.* Front Cell Neurosci, 2014. **8**: p. 314.

53. Thumkeo, D., S. Watanabe, and S. Narumiya, *Physiological roles of Rho and Rho effectors in mammals.* Eur J Cell Biol, 2013. **92**(10-11): p. 303-15.

54. Zhang, X., et al., *Involvement of RhoA/ROCK Signaling in Aβ-Induced Chemotaxis, Cytotoxicity and Inflammatory Response of Microglial BV2 Cells.* Cell Mol Neurobiol, 2019. **39**(5): p. 637-650.

55. Minin, A.A., et al., *Regulation of mitochondria distribution by RhoA and formins.* Journal of Cell Science, 2006. **119**(4): p. 659-670.

56. Chen, W., et al., *The role of the RhoA/Rho kinase pathway in angiogenesis and its potential value in prostate cancer (Review).* Oncol Lett, 2014. **8**(5): p. 1907-1911.

57. Bros, M., et al., *RhoA as a Key Regulator of Innate and Adaptive Immunity.* Cells, 2019. **8**(7).

58. Pedersen, E. and C. Brakebusch, *Rho GTPase function in development: how in vivo models change our view.* Exp Cell Res, 2012. **318**(14): p. 1779-87.

59. Zhou, X. and Y. Zheng, *Cell type-specific signaling function of RhoA GTPase: lessons from mouse gene targeting.* J Biol Chem, 2013. **288**(51): p. 36179-88.

60. Nunes, K.P., C.S. Rigsby, and R.C. Webb, *RhoA/Rho-kinase and vascular diseases: what is the link?* Cellular and Molecular Life Sciences, 2010. **67**(22): p. 3823-3836.

61. Kilian, L.S., D. Frank, and A.Y. Rangrez, *RhoA Signaling in Immune Cell Response and Cardiac Disease.* Cells, 2021. **10**(7): p. 1681.

62. Orgaz, J.L., C. Herraiz, and V. Sanz-Moreno, *Rho GTPases modulate malignant transformation of tumor cells.* Small GTPases, 2014. **5**: p. e29019.

63. Crosas-Molist, E., et al., *Rho GTPase signaling in cancer progression and dissemination.* Physiol Rev, 2022. **102**(1): p. 455-510.

64. Rodrigues, P., et al., *RHOA inactivation enhances Wnt signalling and promotes colorectal cancer.* Nat Commun, 2014. **5**: p. 5458.

65. Zandvakili, I., et al., *Loss of RhoA Exacerbates, Rather Than Dampens, Oncogenic K-Ras Induced Lung Adenoma Formation in Mice.* PLoS One, 2015. **10**(6): p. e0127923.

66. Svensmark, J.H. and C. Brakebusch, *Rho GTPases in cancer: friend or foe?* Oncogene, 2019. **38**(50): p. 7447-7456.

67. Bustelo, X.R., *RHO GTPases in cancer: known facts, open questions, and therapeutic challenges.* Biochem Soc Trans, 2018. **46**(3): p. 741-760.

68. Kataoka, K. and S. Ogawa, *Variegated RHOA mutations in human cancers.* Exp Hematol, 2016. **44**(12): p. 1123-1129.

69. Schaefer, A. and C.J. Der, *RHOA takes the RHOad less traveled to cancer*. Trends Cancer, 2022. **8**(8): p. 655-669.

70. Mayer, T., et al., *A mutant form of the rho protein can restore stress fibers and adhesion plaques in v-src transformed fibroblasts.* Oncogene, 1999. **18**(12): p. 2117-2128.

71. Michaelson, D., et al., *Differential Localization of Rho Gtpases in Live Cells.* Journal of Cell Biology, 2001. **152**(1): p. 111-126.

72. Chen, S., et al., *Activation Mechanism of RhoA Caused by Constitutively Activating Mutations G14V and Q63L.* International Journal of Molecular Sciences, 2022. **23**(24): p. 15458.

73. Kakiuchi, M., et al., *Recurrent gain-of-function mutations of RHOA in diffuse-type gastric carcinoma.* Nat Genet, 2014. **46**(6): p. 583-7.

74. Wang, K., et al., *Whole-genome sequencing and comprehensive molecular profiling identify new driver mutations in gastric cancer.* Nat Genet, 2014. **46**(6): p. 573-82.

75. O'Hayre, M., et al., *Inactivating mutations in GNA13 and RHOA in Burkitt's lymphoma and diffuse large B-cell lymphoma: a tumor suppressor function for the Gα13/RhoA axis in B cells.* Oncogene, 2016. **35**(29): p. 3771-80.

76. Rohde, M., et al., *Recurrent RHOA mutations in pediatric Burkitt lymphoma treated according to the NHL-BFM protocols.* Genes Chromosomes Cancer, 2014. **53**(11): p. 911-6.

77. Nishizawa, T., et al., *DGC-specific RHOA mutations maintained cancer cell survival and promoted cell migration via ROCK inactivation.* Oncotarget, 2018. **9**(33): p. 23198-23207.

78. Zhang, H., et al., *Gain-of-Function RHOA Mutations Promote Focal Adhesion Kinase Activation and Dependency in Diffuse Gastric Cancer.* Cancer Discov, 2020. **10**(2): p. 288-305.

79. Nishizawa, T., et al., *In vivo effects of mutant RHOA on tumor formation in an orthotopic inoculation model.* Oncol Rep, 2019. **42**(5): p. 1745-1754.

80. Lohr, J.G., et al., *Discovery and prioritization of somatic mutations in diffuse large B-cell lymphoma (DLBCL) by whole-exome sequencing.* Proc Natl Acad Sci U S A, 2012. **109**(10): p. 3879-84.

81. Cho, S.Y., et al., *Sporadic Early-Onset Diffuse Gastric Cancers Have High Frequency of Somatic CDH1 Alterations, but Low Frequency of Somatic RHOA Mutations Compared With Late-Onset Cancers.* Gastroenterology, 2017. **153**(2): p. 536-549.e26.

82. Sakata-Yanagimoto, M., et al., *Somatic RHOA mutation in angioimmunoblastic T cell lymphoma.* Nat Genet, 2014. **46**(2): p. 171-5.

83. Palomero, T., et al., *Recurrent mutations in epigenetic regulators, RHOA and FYN kinase in peripheral T cell lymphomas.* Nat Genet, 2014. **46**(2): p. 166-70.

84. Chiba, S., et al., *G17V RHOA: Genetic evidence of GTP-unbound RHOA playing a role in tumorigenesis in T cells.* Small GTPases, 2015. **6**(2): p. 100-3.

85. Yoo, H.Y., et al., *A recurrent inactivating mutation in RHOA GTPase in angioimmunoblastic T cell lymphoma.* Nat Genet, 2014. **46**(4): p. 371-5.

86. Zang, S., et al., *Mutations in 5-methylcytosine oxidase TET2 and RhoA cooperatively disrupt T cell homeostasis.* J Clin Invest, 2017. **127**(8): p. 2998-3012.

87. Ng, S.Y., et al., *RhoA G17V is sufficient to induce autoimmunity and promotes T-cell lymphomagenesis in mice.* Blood, 2018. **132**(9): p. 935-947.

88. Cortes, J.R., et al., *RHOA G17V Induces T Follicular Helper Cell Specification and Promotes Lymphomagenesis.* Cancer Cell, 2018. **33**(2): p. 259-273.e7.

89. Nagata, Y., et al., *Variegated RHOA mutations in adult T-cell leukemia/lymphoma.* Blood, 2016. **127**(5): p. 596-604.

90. Kumar, B.V., T.J. Connors, and D.L. Farber, *Human T Cell Development, Localization, and Function throughout Life.* Immunity, 2018. **48**(2): p. 202-213.

91. Sallusto, F., *Heterogeneity of Human CD4(+) T Cells Against Microbes.* Annu Rev Immunol, 2016. **34**: p. 317-34.

92. Golubovskaya, V. and L. Wu, *Different Subsets of T Cells, Memory, Effector Functions, and CAR-T Immunotherapy.* Cancers, 2016. **8**(3): p. 36.

93. Dustin, M.L., *The immunological synapse.* Cancer Immunol Res, 2014. **2**(11): p. 1023-33.

94. Hwang, J.R., et al., *Recent insights of T cell receptor-mediated signaling pathways for T cell activation and development.* Exp Mol Med, 2020. **52**(5): p. 750-761.

95. Shah, K., et al., *T cell receptor (TCR) signaling in health and disease.* Signal Transduct Target Ther, 2021. **6**(1): p. 412.

96. Palacios, E.H. and A. Weiss, *Function of the Src-family kinases, Lck and Fyn, in T-cell development and activation.* Oncogene, 2004. **23**(48): p. 7990-8000.

97. Samelson, L.E., *Signal transduction mediated by the T cell antigen receptor: the role of adapter proteins.* Annu Rev Immunol, 2002. **20**: p. 371-94.

98. Téllez, C.N., et al., *T-cell activation, alterations in systemic lupus erythematosus: A narrative review.* Revista Colombiana de Reumatología (English Edition), 2018. **25**(1): p. 38-54.

99. Mastrogiovanni, M., et al., *Coordinating Cytoskeleton and Molecular Traffic in T Cell Migration, Activation, and Effector Functions.* Front Cell Dev Biol, 2020. **8**: p. 591348.

100. Saoudi, A., et al., *Rho-GTPases as key regulators of T lymphocyte biology.* Small GTPases, 2014. **5**.

101. Zanin-Zhorov, A., M.L. Dustin, and B.R. Blazar, *PKC-θ function at the immunological synapse: prospects for therapeutic targeting.* Trends in Immunology, 2011. **32**(8): p. 358-363.

102. Trebak, M. and J.P. Kinet, *Calcium signalling in T cells.* Nat Rev Immunol, 2019. **19**(3): p. 154-169.

103. Courtney, A.H., W.L. Lo, and A. Weiss, *TCR Signaling: Mechanisms of Initiation and Propagation.* Trends Biochem Sci, 2018. **43**(2): p. 108-123.

104. Feske, S., *Calcium signalling in lymphocyte activation and disease.* Nature Reviews Immunology, 2007. **7**(9): p. 690-702.

105. Braiman, A., et al., *Recruitment and activation of PLCgamma1 in T cells: a new insight into old domains.* EMBO J, 2006. **25**(4): p. 774-84.

106. Iqbal, J., et al., *Molecular and Genomic Landscape of Peripheral T-Cell Lymphoma.* Cancer Treat Res, 2019. **176**: p. 31-68.

107. Zhang, Y., et al., *Genomics of Peripheral T-Cell Lymphoma and Its Implications for Personalized Medicine.* Front Oncol, 2020. **10**: p. 898.

108. Alaggio, R., et al., *The 5th edition of the World Health Organization Classification of Haematolymphoid Tumours: Lymphoid Neoplasms.* Leukemia, 2022. **36**(7): p. 1720-1748.

109. Fiore, D., et al., *Peripheral T cell lymphomas: from the bench to the clinic.* Nat Rev Cancer, 2020. **20**(6): p. 323-342.

110. Zettl, A., et al., *Genomic Profiling of Peripheral T-Cell Lymphoma, Unspecified, and Anaplastic Large T-Cell Lymphoma Delineates Novel Recurrent Chromosomal Alterations.* The American Journal of Pathology, 2004. **164**(5): p. 1837-1848.

111. Heavican, T.B., et al., *Genetic drivers of oncogenic pathways in molecular subgroups of peripheral T-cell lymphoma.* Blood, 2019. **133**(15): p. 1664-1676.

112. Morris, S.W., et al., *Fusion of a kinase gene, ALK, to a nucleolar protein gene, NPM, in non-Hodgkin's lymphoma.* Science, 1994. **263**(5151): p. 1281-4.

113. Vallois, D., et al., *Activating mutations in genes related to TCR signaling in angioimmunoblastic and other follicular helper T-cell-derived lymphomas.* Blood, 2016. **128**(11): p. 1490-502.

114. Rohr, J., et al., *Recurrent activating mutations of CD28 in peripheral T-cell lymphomas.* Leukemia, 2016. **30**(5): p. 1062-70.

115. Kataoka, K., et al., *Integrated molecular analysis of adult T cell leukemia/lymphoma.* Nature Genetics, 2015. **47**(11): p. 1304-1315.

116. Fujisawa, M., et al., *Activation of RHOA-VAV1 signaling in angioimmunoblastic T-cell lymphoma.* Leukemia, 2018. **32**(3): p. 694-702.

117. Robles-Valero, J., et al., *Cancer-associated mutations in VAV1 trigger variegated signaling outputs and T-cell lymphomagenesis.* EMBO J, 2021. **40**(22): p. e108125.

118. Boddicker, R.L., G.L. Razidlo, and A.L. Feldman, *Genetic alterations affecting GTPases and T-cell receptor signaling in peripheral T-cell lymphomas.* Small GTPases, 2019. **10**(1): p. 33-39.

119. Pechloff, K., et al., *The fusion kinase ITK-SYK mimics a T cell receptor signal and drives oncogenesis in conditional mouse models of peripheral T cell lymphoma.* J Exp Med, 2010. **207**(5): p. 1031-44.

120. Drieux, F., et al., *Detection of Gene Fusion Transcripts in Peripheral T-Cell Lymphoma Using a Multiplexed Targeted Sequencing Assay.* J Mol Diagn, 2021. **23**(8): p. 929-940.

121. Abate, F., et al., *Activating mutations and translocations in the guanine exchange factor VAV1 in peripheral T-cell lymphomas.* Proc Natl Acad Sci U S A, 2017. **114**(4): p. 764-769.

122. Boddicker, R.L., et al., *Integrated mate-pair and RNA sequencing identifies novel, targetable gene fusions in peripheral T-cell lymphoma.* Blood, 2016. **128**(9): p. 1234-45.

123. Kogure, Y. and K. Kataoka, *Genetic alterations in adult T-cell leukemia/lymphoma.* Cancer Sci, 2017. **108**(9): p. 1719-1725.

124. Waldmann, T.A. and J. Chen, *Disorders of the JAK/STAT Pathway in T Cell Lymphoma Pathogenesis: Implications for Immunotherapy.* Annu Rev Immunol, 2017. **35**: p. 533-550.

125. Watanabe, M., et al., *JunB induced by constitutive CD30-extracellular signal-regulated kinase 1/2 mitogen-activated protein kinase signaling activates the CD30 promoter in anaplastic large cell lymphoma and reed-sternberg cells of Hodgkin lymphoma.* Cancer Res, 2005. **65**(17): p. 7628-34.

126. da Silva Almeida, A.C., et al., *The mutational landscape of cutaneous T cell lymphoma and Sézary syndrome.* Nat Genet, 2015. **47**(12): p. 1465-70.

127. Wang, M., et al., *Angioimmunoblastic T cell lymphoma: novel molecular insights by mutation profiling.* Oncotarget, 2017. **8**(11): p. 17763-17770.

128. Marçais, A., et al., *Adult T cell leukemia aggressivenness correlates with loss of both 5-hydroxymethylcytosine and TET2 expression.* Oncotarget, 2017. **8**(32): p. 52256-52268.

129. Cairns, R.A., et al., *IDH2 mutations are frequent in angioimmunoblastic T-cell lymphoma.* Blood, 2012. **119**(8): p. 1901-3.

130. Wang, C., et al., *IDH2R172 mutations define a unique subgroup of patients with angioimmunoblastic T-cell lymphoma.* Blood, 2015. **126**(15): p. 1741-52.

131. Kim, T.Y., et al., *Impact of Epstein-Barr Virus on Peripheral T-Cell Lymphoma Not Otherwise Specified and Angioimmunoblastic T-Cell Lymphoma.* Front Oncol, 2021. **11**: p. 797028.

132. Watanabe, T., *Adult T-cell leukemia: molecular basis for clonal expansion and transformation of HTLV-1-infected T cells.* Blood, 2017. **129**(9): p. 1071-1081.

133. Portis, T., et al., *Analysis of p53 Inactivation in a Human T-Cell Leukemia Virus Type 1 Tax Transgenic Mouse Model.* Journal of Virology, 2001. **75**(5): p. 2185-2193.

134. Timmins, M.A., S.D. Wagner, and M.J. Ahearne, *The new biology of PTCL-NOS and AITL: current status and future clinical impact.* Br J Haematol, 2020. **189**(1): p. 54-66.

135. Mohammed Saleh, M.F., et al., *Recent Advances in Diagnosis and Therapy of Angioimmunoblastic T Cell Lymphoma.* Curr Oncol, 2021. **28**(6): p. 5480-5498.

136. Mhaidly, R., et al., *New preclinical models for angioimmunoblastic T-cell lymphoma: filling the GAP*. Oncogenesis, 2020. **9**(8): p. 73.

137. Ganapathi, K.A., K.H. Karner, and M.P. Menon, *Peripheral T-Cell Lymphomas of the T Follicular Helper Type: Clinical, Pathological, and Genetic Attributes*. Hemato, 2022. **3**(1): p. 268-286.

138. Lewis, N.E., R. Sardana, and A. Dogan, *Mature T-cell and NK-cell lymphomas: updates on molecular genetic features.* Int J Hematol, 2023.

139. Federico, M., et al., *Clinicopathologic Characteristics of Angioimmunoblastic T-Cell Lymphoma: Analysis of the International Peripheral T-Cell Lymphoma Project.* Journal of Clinical Oncology, 2013. **31**(2): p. 240-246.

140. Crotty, S., *T Follicular Helper Cell Differentiation, Function, and Roles in Disease.* Immunity, 2014. **41**(4): p. 529-542.

141. Gaulard, P. and L. de Leval, *The microenvironment in T-cell lymphomas: emerging themes.* Semin Cancer Biol, 2014. **24**: p. 49-60.

142. Scourzic, L., et al., *DNMT3A(R882H) mutant and Tet2 inactivation cooperate in the deregulation of DNA methylation control to induce lymphoid malignancies in mice.* Leukemia, 2016. **30**(6): p. 1388-98.

143. Yoo, H.Y., et al., *Frequent CTLA4-CD28 gene fusion in diverse types of T-cell lymphoma.* Haematologica, 2016. **101**(6): p. 757-63.

144. Yao, W.Q., et al., *Angioimmunoblastic T-cell lymphoma contains multiple clonal T-cell populations derived from a common TET2 mutant progenitor cell.* J Pathol, 2020. **250**(3): p. 346-357.

145. Lage, L.A.P.C., et al., *Angioimmunoblastic T-cell lymphoma and correlated neoplasms with T-cell follicular helper phenotype: from molecular mechanisms to therapeutic advances.* Front Oncol, 2023. **13**: p. 1177590.

146. Sibon, D., *Peripheral T-Cell Lymphomas: Therapeutic Approaches.* Cancers, 2022. **14**(9): p. 2332.

147. Tari, G., F. Lemonnier, and F. Morschhauser, *Epigenetic focus on angioimmunoblastic T-cell lymphoma: pathogenesis and treatment.* Curr Opin Oncol, 2021. **33**(5): p. 400-405.

148. Moskowitz, A.J., *Practical Treatment Approach for Angioimmunoblastic T-Cell Lymphoma.* Journal of Oncology Practice, 2019. **15**(3): p. 137-143.

149. Mortlock, D., et al., *High efficiency transfection of monkey kidney COS-1 cells.* Journal of Tissue Culture Methods, 1993. **15**(4): p. 176-180.

150. Heukeshoven, J. and R. Dernick, *Simplified method for silver staining of proteins in polyacrylamide gels and the mechanism of silver staining.* ELECTROPHORESIS, 1985. **6**(3): p. 103-112.

151. Shevchenko, A., et al., *Mass Spectrometric Sequencing of Proteins from Silver-Stained Polyacrylamide Gels.* Analytical Chemistry, 1996. **68**(5): p. 850-858.

152. Rappsilber, J., M. Mann, and Y. Ishihama, *Protocol for micro-purification, enrichment, pre-fractionation and storage of peptides for proteomics using StageTips.* Nat Protoc, 2007. **2**(8): p. 1896-906.

153. Cox, J. and M. Mann, *MaxQuant enables high peptide identification rates, individualized p.p.b.-range mass accuracies and proteome-wide protein quantification.* Nat Biotechnol, 2008. **26**(12): p. 1367-72.

154. Schwanhäusser, B., et al., *Global quantification of mammalian gene expression control.* Nature, 2011. **473**(7347): p. 337-42.

155. Cheng, Z., et al., *Luciferase Reporter Assay System for Deciphering GPCR Pathways.* Curr Chem Genomics, 2010. **4**: p. 84-91.

156. Hill, C.S., J. Wynne, and R. Treisman, *The Rho family GTPases RhoA, Rac1, and CDC42Hs regulate transcriptional activation by SRF.* Cell, 1995. **81**(7): p. 1159-70.

157. Barreira, M., et al., *The C-terminal SH3 domain contributes to the intramolecular inhibition of Vav family proteins.* Sci Signal, 2014. **7**(321): p. ra35.

158. Pizzi, M., E. Margolskee, and G. Inghirami, *Pathogenesis of Peripheral T Cell Lymphoma.* Annual Review of Pathology: Mechanisms of Disease, 2018. **13**(1): p. 293-320.

159. Bigas, A., et al., *Recent advances in T-cell lymphoid neoplasms.* Exp Hematol, 2022. **106**: p. 3-18.

160. Schuld, N.J., et al., *The chaperone protein SmgGDS interacts with small GTPases entering the prenylation pathway by recognizing the last amino acid in the CAAX motif.* J Biol Chem, 2014. **289**(10): p. 6862-6876.

161. Lanning, C.C., R. Ruiz-Velasco, and C.L. Williams, *Novel mechanism of the co-regulation of nuclear transport of SmgGDS and Rac1.* J Biol Chem, 2003. **278**(14): p. 12495-506.

162. Clipstone, N.A. and G.R. Crabtree, *Identification of calcineurin as a key signalling enzyme in T-lymphocyte activation.* Nature, 1992. **357**(6380): p. 695-7.

163. Philip, M., et al., *Chromatin states define tumour-specific T cell dysfunction and reprogramming.* Nature, 2017. **545**(7655): p. 452-456.

164. Gao, X., et al., *Notch Signaling Promotes Mature T-Cell Lymphomagenesis.* Cancer Res, 2022. **82**(20): p. 3763-3773.

165. Vaqué, J.P., et al., *PLCG1 mutations in cutaneous T-cell lymphomas.* Blood, 2014. **123**(13): p. 2034-43.

166. Cortes, J.R., et al., *Oncogenic Vav1-Myo1f induces therapeutically targetable macrophage-rich tumor microenvironment in peripheral T cell lymphoma.* Cell Rep, 2022. **39**(3): p. 110695.

167. Rodriguez Cortes, J., et al., *Role of Vav1 Genomic Alterations in T-Cell Differentiation and Transformation in Peripheral T-Cell Lymphoma.* Blood, 2019. **134**(Supplement_1): p. 1482-1482.

168. Crespo, P., et al., *Phosphotyrosine-dependent activation of Rac-1 GDP/GTP exchange by the vav proto-oncogene product.* Nature, 1997. **385**(6612): p. 169-172.

169. Zhi, H., et al., *SmgGDS is up-regulated in prostate carcinoma and promotes tumour phenotypes in prostate cancer cells.* J Pathol, 2009. **217**(3): p. 389-97.

170. Tew, G.W., et al., *SmgGDS regulates cell proliferation, migration, and NF-kappaB transcriptional activity in non-small cell lung carcinoma.* J Biol Chem, 2008. **283**(2): p. 963-76.

171. Hauser, A.D., et al., *The SmgGDS splice variant SmgGDS-558 is a key promoter of tumor growth and RhoA signaling in breast cancer.* Mol Cancer Res, 2014. **12**(1): p. 130-42.

172. Bergom, C., et al., *The tumor-suppressive small GTPase DiRas1 binds the noncanonical guanine nucleotide exchange factor SmgGDS and antagonizes SmgGDS interactions with oncogenic small GTPases.* J Biol Chem, 2016. **291**(20): p. 10948.

173. Schuld, N.J., et al., *SmgGDS-558 regulates the cell cycle in pancreatic, non-small cell lung, and breast cancers.* Cell Cycle, 2014. **13**(6): p. 941-52.

174. Brandt, A.C., et al., *Splice switching an oncogenic ratio of SmgGDS isoforms as a strategy to diminish malignancy.* Proc Natl Acad Sci U S A, 2020. **117**(7): p. 3627-3636.

175. Strassheim, D., et al., *Unique in vivo associations with SmgGDS and RhoGDI and different guanine nucleotide exchange activities exhibited by RhoA, dominant*

negative RhoA(Asn-19), and activated RhoA(Val-14). J Biol Chem, 2000. **275**(10): p. 6699-702.

176. Chen, G., et al., *Characterization of a novel CRAC inhibitor that potently blocks human T cell activation and effector functions.* Mol Immunol, 2013. **54**(3-4): p. 355-67.

APPENDIX

Resumen en español

RESUMEN DE LA INTRODUCCIÓN

RHOA

RHOA es una proteína perteneciente a la familia de las proteínas RHO GTPasas que actúa como un interruptor molecular, fluctuando entre un estado activo cuando está unida a GTP, e inactivo cuando está unida a GDP. Su ciclo de activación e inactivación está altamente regulado por proteínas que catalizan el intercambio de GDP por GTP (GEFs) y por proteínas que promueven la hidrólisis de GTP a GDP (GAPs). Además, existen inhibidores de la disociación de nucleótidos de guanina (GDIs), que impiden la activación de RHOA al secuestrarlo en el citosol. Una vez activada, RHOA interactúa con diferentes proteínas efectoras para regular una amplia gama de funciones celulares. RHOA desempeña un papel crucial en la regulación de diversos procesos celulares, como por ejemplo la progresión del ciclo y división celulares, la expresión génica, el transporte vesicular, migración, morfogénesis o adhesión, entre otras.

La desregulación de RHOA se ha asociado con una amplia gama de enfermedades patológicas debido a su participación en procesos celulares y biológicos vitales, incluido en cáncer. RHOA ha sido implicada en casi todas las etapas de la tumorigénesis, actuando como un oncogén en varios tipos de tumores. Sin embargo, la visión convencional de que RHOA actúa exclusivamente como un oncogén está cambiando en los últimos años. Estudios en modelos de ratones de cáncer de colon y adenocarcinomas de pulmón demostraron que la inhibición de RhoA resultó en un mayor crecimiento tumoral. Además, se ha observado que la pérdida de *RhoA* exacerba la formación de adenocarcinomas pulmonares inducidos por K-Ras en ratones. Estos hallazgos sugieren que la función de RHOA en tumorigénesis es más compleja de lo que se creía.

Diversas mutaciones se han encontrado en el gen *RHOA* en diversos tipos de tumores, siendo más comunes en linfomas de células T periféricas, cáncer gástrico, cáncer de vejiga y linfomas de células B. Estas mutaciones afectan principalmente a los dominios de unión al GTP y los dominios de cambio de la proteína. Algunas mutaciones en *RHOA* activan su función oncogénica, pero también se han encontrado mutaciones que resultan en pérdida de función. Estas mutaciones tienen un impacto diverso en diferentes tumores y su papel en el desarrollo tumoral requiere una mayor investigación.

Entre las mutaciones más frecuentes se encuentra la mutación G17V, que se ha encontrado en linfomas de células T periféricas, especialmente en linfomas T angioinmunoblásticos. Esta mutación es una mutación de pérdida de función que inactiva la vía de señalización de RHOA. Otras mutaciones afectan los residuos Tyr42 y Arg5, y su impacto en la tumorigénesis varía dependiendo del tipo de tumor y el tipo de mutación.

En resumen, las mutaciones en *RHOA* desempeñan un papel complejo en la tumorigénesis y su efecto en el desarrollo tumoral varía dependiendo del tipo de mutación y el tipo de tumor. Aunque se ha caracterizado un número limitado de mutaciones en *RHOA*, muchas mutaciones aún no se han estudiado y se desconocen sus efectos. Se requiere más investigación para comprender completamente el papel de las mutaciones de *RHOA* en cáncer.

Linfomas de células T periféricos

Los linfomas de células T periféricas son un grupo de malignidades raras y altamente heterogéneas que se originan en células T y NK maduras. Constituyen aproximadamente el 10-15% de todos los linfomas no Hodgkin en los países occidentales y alrededor del 20-30% en Asia y América del Sur. El trastorno más común es el linfoma de células T periférico no especificado (PTCL-NOS), que comprende aproximadamente el 30% de los linfomas de células T periféricas. Otros subtipos incluyen el linfoma angioinmunoblástico de células T (AITL), el linfoma anaplásico de células grandes (ALCL) y el linfoma de células T natural/linfoma de células T extranodal de linaje NK (ENKTCL), que representan aproximadamente el 10-30%, 15% y 5-6% de los casos, respectivamente.

En cuanto a los linfomas de células T angioinmunoblásticos, se trata de la segunda subcategoría más prevalente de los linfomas de células T y NK, representando entre el 15% y el 30% de los casos. La incidencia de AITL varía geográficamente, siendo Europa la región con mayor frecuencia (29%), seguida de Asia (18%) y Estados Unidos (16%). Esta enfermedad se desarrolla en etapas tardías de la vida, con una edad promedio de inicio de 69 años, y la mayoría de los pacientes son diagnosticados en etapas avanzadas de la enfermedad (hasta un 80%). Como resultado, la tasa de supervivencia general es baja, con una mediana de supervivencia de 5 años y solo el 32% de los pacientes sobreviven más allá de ese período.

Los pacientes con AITL suelen presentar hepatomegalia, esplenomegalia, linfadenopatía difusa y erupciones cutáneas. Además, los pacientes con AITL a menudo sufren infección por el virus de Epstein-Barr, disfunción inmunológica e inmunodeficiencia. Los ganglios linfáticos muestran una pérdida de la arquitectura con proliferación de venas endoteliales y redes de células dendríticas foliculares expandidas. Las células T neoplásicas expresan marcadores de células T foliculares como PD1, ICOS, CXCR5 y BCL6, postulándose este subconjunto específico de células como la célula de origen de AITL.

El uso de la secuenciación de próxima generación ha permitido la identificación de mutaciones recurrentes en AITL. Las mutaciones más frecuentes afectan a los modificadores epigenéticos *TET2, DNMT3A* e *IDH2*, así como a *RHOA*, que a menudo co-ocurren. Las mutaciones inactivadoras de *TET2* están presentes en hasta el 80% de los casos de AITL y promueven la hipermetilación del ADN y la regulación anormal de la expresión génica. Las mutaciones de *RHOA* están presentes en el 50-70% de los casos, siendo la mutación G17V la más prevalente. Esta mutación co-ocurre exclusivamente con mutaciones en *TET2*, con o sin mutaciones en *IDH2*. Además, se ha observado la pérdida simultánea de *TET2* y *DNMT3A* en AITL. Además, los pacientes con AITL a menudo presentan mutaciones en componentes de la vía de señalización del TCR, incluyendo mutaciones en los genes *PLCG1, CD28, VAV1* y *FYN*, o fusiones génicas que afectan a genes como *VAV1, CD28* o *CTLA4*.

El tratamiento de primera línea actual para este tipo de linfomas se basa en agentes quimioterapéuticos como CHOP. Sin embargo, las tasas de recaída son altas. Se han investigado alternativas como CHOEP, DA-EPOCH y HyperCVAD, quimioterapia seguida de trasplante autólogo de células madre, y terapias inmunológicas combinadas con CHOP, pero no han mostrado mejores resultados. Además, se han propuesto medicamentos que actúan sobre la epigenética, como inhibidores de histona deacetilasa y agentes hipometilantes, con resultados prometedores en AITL refractarios. También se han estudiado terapias dirigidas a vías de señalización específicas, como inhibidores de PI3K, inhibidores de quinasas e inhibidores de la vía JAK/STAT.

En resumen, la falta de tratamientos efectivos para AITL destaca la necesidad de más investigación. La combinación de enfoques epigenéticos y de señalización de células T podría ser una estrategia prometedora para AITL y otros PTCL.

Por todo lo expuesto anteriormente, este trabajo tiene los siguientes objetivos generales:

1. Caracterizar las mutaciones del gen *RHOA* descritas en tumores humanos.
2. Comprender los programas mecanísticos y patobiológicos desencadenados por las mutaciones de *RHOA* en los linfomas de células T periféricas.
3. Obtener nuevos conocimientos terapéuticos para el tratamiento de los linfomas de células T periféricas impulsados por *RHOA*^{G17V}.

RESUMEN DE LOS RESULTADOS

Caracterización de las mutaciones de RHOA asociadas a tumores

En este estudio se caracterizaron las mutaciones asociadas a *RHOA* en tumores. Se realizaron ensayos utilizando luciferasa para evaluar el efecto de las mutaciones en la actividad canónica de RHOA, encontrando que las mutaciones de RHOA pueden clasificarse en tres categorías funcionales: mutaciones similares a WT, mutaciones de ganancia de función (GOF) y mutaciones de pérdida de función (LOF). En cuanto a la localización en la estructura de la proteína, la mayoría de las mutaciones ubicadas en los dominios de cambio fueron principalmente LOF, mientras que las mutaciones ubicadas en los dominios de unión al GTP podrían exhibir efectos tanto GOF como LOF.

Dado que las mutaciones de *RHOA* relacionadas con PTCL mostraron efectos canónicos opuestos incluso dentro del mismo tipo de tumor, se investigó si estas mutaciones pudieran desencadenar funciones no exploradas. Para ello, se realizaron ensayos de luciferasa para analizar el efecto de estas mutaciones en la activación de rutas de señalización hiperactivadas en PTCL, incluyendo STAT3, NOTCH1, NF-κB, y AP-1. Se comprobó que la activación de estas vías de señalización no depende de la actividad GTPasa de RHOA, indicando que estas mutaciones no promueven linfomagénesis a través de estos mecanismos específicos. Sin embargo, se descubrió que las mutaciones relacionadas con linfomas de células T periféricos muestran una función neomórfica (NEO), activando la vía de señalización de NFAT independientemente de su actividad canónica. Además, esta nueva función es específica de RHOA, pero no de otras GTPasas como RAC1 y CDC42.

Además, se determinó que la activación de NFAT por las mutaciones requiere la entrada de calcio desde fuera de la célula, en lugar de depender solo del calcio almacenado en el retículo endoplasmático.

Los mutantes neomórficos de RHOA activan NFAT a través de LAT, PLCγ1 y SLP76

Se llevó a cabo un estudio para investigar qué proteínas relacionadas con el TCR son esenciales para la activación de NFAT mediada por los mutantes neomórficos. Los resultados mostraron que el impacto de las mutaciones neomórficas en la activación de NFAT depende de la presencia de las proteínas LAT, PLCγ1 y SLP76, y no se ve influenciado por VAV1. Además, mediante ensayos de co-inmunoprecipitación se comprobó que solo los mutantes neomórficos $RHOA^{C16R}$ y $RHOA^{G17V}$ interactúa con las proteínas PLCγ1, VAV1 y SLP76, mientras que $RHOA^{WT}$ no lo hace. Estos hallazgos proporcionan información importante sobre los mecanismos de señalización relacionados con el TCR y la activación de NFAT en las células Jurkat.

RAP1GDS1 media el efecto neomórfico de RHOA

Dado que las mutaciones NEO de *RHOA* promueven la activación de NFAT incluso cuando muestran una actividad canónica opuesta, se llevaron a cabo ensayos de proteómica para investigar las interacciones y los mecanismos de activación de la vía NFAT por las mutaciones neomórficas de *RHOA* en células Jurkat. Se descubrió que estas mutaciones interactuaban de manera diferente con las proteínas RHOGDIα y RAP1GDS1. Mientras que $RHOA^{WT}$ interactuaba fuertemente con RHOGDIα, las mutaciones neomórficas mostraron una fuerte interacción con RAP1GDS1. Estos resultados indican que RAP1GDS1 desempeña un papel crucial en la activación de la vía NFAT por las mutaciones neomórficas de *RHOA*.

Con el fin de comprobar si estas interacciones eran específicas de mutaciones neomórficas, se realizaron ensayos de coinmunoprecipitación y se encontró que las mutaciones NEO interactuaban más con RAP1GDS1, mientras que su interacción con RHOGDIα disminuía o se perdía. Además, se examinó la interacción entre RHOA y RAP1GDS1 en comparación con otras proteínas GTPasas como RAC1 y CDC42. se demostró que las mutaciones neomórficas de RHOA interactuaban de manera selectiva con RAP1GDS1 en comparación con otras proteínas GTPasas como RAC1 y CDC42.

Para confirmar el papel de RAP1GDS1 en la activación de NFAT por las mutaciones de RHOA, se llevaron a cabo diferentes estrategias. (1) Se generaron clones celulares en los que se eliminó la expresión endógena de RAP1GDS1 en células Jurkat, demostrando que la eliminación de RAP1GDS1 abolió la activación de NFAT en presencia de las mutaciones de RHOA. (2) Se combinaron las mutaciones NEO de RHOA con mutaciones que interrumpen por completo la interacción con RAP1GDS1, observándose que solo los dobles mutantes $RHOA^{C16R+Y66N}$, $RHOA^{C16R+L69R}$ y $RHOA^{G17V+Y66N}$ fueron incapaces de activar NFAT, así como de interaccionar con RAP1GDS1. (3) Se modificó el dominio CAAX de las proteínas mutantes de RHOA, comprobando que las mutaciones NEO que carecían del dominio CAAX pierden la capacidad de activar NFAT, mientras que las mutaciones que contienen una serina en lugar de una cisteína en el dominio CAAX (versiones SAAL) aún conservan la capacidad de activar esta vía. Se comprobó la interacción de estas versiones del dominio CAAX con ambas isoformas de RAP1GDS1 y se observó que cuando se elimina el dominio CAAX los mutantes pierden la interacción con ambas isoformas de RAP1GDS1, mientras que las versiones SAAL conservan su interacción exclusivamente con RAP1GDS1-607. Además, se descubrió que la pérdida de interacción entre RHOA y RHOGDIα aumentaba la interacción entre RHOA y RAP1GDS1, lo que permitía que una mutación no neomórfica ($RHOA^{R5W}$) tuviera un efecto neomórfico en la activación de NFAT.

Por último, se investigó la interacción del complejo RHOA-RAP1GDS1 con las proteínas PLCγ1, SLP76 y VAV1, y se encontró que la pérdida de interacción con RAP1GDS1 disminuía significativamente la interacción con estas proteínas. Estos hallazgos destacan el papel crucial de la interacción entre RHOA y RAP1GDS1 en la regulación de la activación de NFAT.

Papel de las mutaciones neomórficas de *RHOA in vivo*

En primer lugar, se llevó a cabo un estudio de los efectos tempranos de estas mutaciones en células T primarias. Los hallazgos iniciales mostraron que la expresión a corto plazo de las mutaciones neomórficas de *RHOA* por sí solas no mejoraba la proliferación ni inducía la activación de las células T $CD4^+$. Sin embargo, en ausencia de *TET2*, solo los mutantes de pérdida de función $RHOA^{G17V}$ y $RHOA^{A161E}$ aumentaron los niveles de proliferación de células T $CD4^+$, así como los niveles de p-Erk1/2 y p-S6. Estos resultados sugirieron un fuerte efecto sinérgico de las mutaciones neomórficas de pérdida de función

de *RHOA* y la pérdida de *TET2* en las células T $CD4^+$, lo cual es consistente con el patrón de mutaciones observado en pacientes con AITL.

Mientras que las células Jurkat demostraron el papel crucial de esta interacción, no todas las mutaciones neomórficas de *RHOA* mostraron un aumento en la proliferación en células T primarias cuando se combinaban con la pérdida de *TET2*, a pesar de su interacción con RAP1GDS1. Para obtener más información al respecto, se examinó el impacto de la expresión de los dobles mutantes que interrumpen la formación del complejo RHOA-RAP1GDS1, así como las versiones CAAL, en células T $CD4^+$. Los resultados mostraron que el doble mutante $RHOA^{G17V+Y66N}$ aumentó la proliferación en el contexto de la pérdida de *TET2*, pero no en la misma medida que $RHOA^{G17V}$. Además, las versiones SAAL de $RHOA^{C16R}$ y $RHOA^{G17V}$ aumentaron significativamente la proliferación en células T $CD4^+$ sin *TET2*, mientras que las versiones ΔCAAL no aumentaron la proliferación. En conjunto, estos resultados confirman y refuerzan hallazgos anteriores, destacando el papel significativo de RAP1GDS1 en la función neomórfica de RHOA en células T.

Se llevaron a cabo experimentos de transferencia adoptiva de células T para investigar la relevancia de las mutaciones RHOA NEO en el desarrollo de enfermedades similares al PTCL en ratones. Se utilizó la mutación $RHOA^{G17V}$, común en AITL, y la mutación $RHOA^{C16R}$, común en ATLL. Se observó que las células que expresaban $RHOA^{G17V}$ inducían la formación de linfomas de tipo T_{FH} y la muerte de los ratones, mientras que las células que expresaban $RHOA^{C16R}$ no mostraron estas características. Estos resultados demuestran que la mutación $RHOA^{G17V}$ promueve la diferenciación de las células T en linfocitos T_{FH} y el desarrollo de AITL en ratones.

Debido a la asociación entre la mutación $RHOA^{G17V}$ y la activación de la vía NFAT en células T, se trataron ratones receptores que expresaban $RHOA^{G17V}$ en células T $CD4^+$ $Tet2^{-/-}$ con un inhibidor de NFAT llamado FK506. El tratamiento redujo la expansión de las células tumorales y disminuyó la expresión de marcadores asociados con el fenotipo T_{FH}. Finalmente, se realizaron experimentos *in vitro* para evaluar el efecto de diferentes inhibidores en células tumorales $Tet2^{-/-}$; $RHOA^{G17V}$. Se probó la inhibición de NFAT, ICOS, PI3K y la señalización de ICN1, comprobando que la inhibición de NFAT tuvo un efecto notable al bloquear la proliferación de las células tumorales y aumentar la apoptosis. Sin embargo, la inhibición de ICOS, PI3K y la señalización de

ICN1 no tuvo un impacto significativo en la viabilidad de las células tumorales. Estos resultados sugieren que el tratamiento con FK506 puede ser efectivo para detener el crecimiento de las células tumorales asociadas con AITL.

CONCLUSIONES

La investigación presentada en esta tesis de doctorado sugiere que, según los hallazgos previos:

1. Las mutaciones de RHOA en los linfomas de células T periféricas muestran un efecto neomórfico que es mediado por:
    a) Prenilación defectuosa
    b) Aumento de la unión de RAP1GDS1
    c) Interacciones dependientes de RAP1GDS1 con el signalosoma de PLCγ1.
2. Los mutantes neomórficos de RHOA promueven la proliferación en células primarias de manera dependiente de RAP1GDS1.
3. La linfomagénesis mediada por $RHOA^{G17V}$ es dependiente de NFAT.